

An OASIS of Lyman- α within a neutral intergalactic desert

Reaffirmed line and blue continuum reveal efficient ionising agents at $z = 13$

Joris Witstok , Stefano Carniani , Peter Jakobsen , Andrew J. Bunker , Alex J. Cameron ,
Francesco D'Eugenio , Kevin Hainline , Jakob M. Helton , et al.

(Full author list and affiliations details can be found after the references)

Received March 20, 2026

ABSTRACT

Galaxy assembly was already well underway in the first 400 Myr of cosmic time, as recently revealed by JWST. However, the contribution of these early galaxies to cosmic reionisation remains uncertain. Here we present new JWST/NIRSpec observations of GS-z13-1-LA obtained as part of the OASIS and JADES programmes, whose combined deep (56 h) NIRSpec/PRISM spectrum confirms the Lyman- α line detection and blue UV continuum at redshift $z = 13.1$ presented in a previous work. The measured Lyman- α emission (rest-frame equivalent width of 66_{-9}^{+10} Å) and steep continuum slope ($\beta_{UV} \approx -3$) point towards GS-z13-1-LA hosting a remarkably hot and powerful ionising source, and allow at most a modest contribution from the nebular continuum. The steep turnover of the continuum is still present, but less pronounced in the new OASIS spectrum. Combined, this implies that ionising photons may escape GS-z13-1-LA at a sufficient rate to weaken the other, still undetected UV lines, and to lead the formation of a small ionised bubble ($R_{ion} \approx 0.2$ pMpc). A yet larger bubble could alleviate the required ionising production efficiency of GS-z13-1-LA from $\xi_{ion} \approx 10^{26.4}$ Hz erg $^{-1}$ down to $\approx 10^{25.9}$ Hz erg $^{-1}$, still extremely high but more readily reconcilable with stellar models. In turn, this would require a notable overdensity of galaxies with highly efficient ionising capabilities, a scenario for which tentative evidence is found in the form of 16 nearby photometric candidates and one spectroscopically confirmed source, JADES-GS-z13-0. The new OASIS observations therefore confirm the overall picture of GS-z13-1-LA as an early beacon of reionisation, providing compelling evidence for its start only 330 Myr after the Big Bang.

Key words. galaxies: high-redshift – dark ages, reionization, first stars – methods: observational

1. Introduction

Most of the baryons in the Universe are contained in the intergalactic medium (IGM; Meiksin 2009). Only a few hundred million years after the Big Bang, neutral atomic hydrogen (H I) within this vast gas reservoir started to be photoionised and heated as a result of the formation of the first astrophysical objects, marking the onset of cosmic reionisation (Dayal & Ferrara 2018).

While future H I 21 cm experiments hold promise to directly trace H I gas in the early Universe (de Lera Acedo et al. 2022), the H I Lyman- α (Ly α) transition is currently the most potent probe of reionisation (see Ouchi et al. 2020 for a review). In its closing stages, corresponding to redshift $z \lesssim 6$, the multitude (‘forest’) of Ly α absorption features observed in quasar spectra is now able to accurately constrain the endpoint of reionisation, which is generally argued to be ‘late’ (persisting down to $z \approx 5.3$; Bosman et al. 2022; Zhu et al. 2022). The Ly α forest even allows the timeline of reionisation to be reconstructed further back in time ($z > 6$) with exquisite precision, although these constraints are subject to model dependency (e.g. Villasenor et al. 2022; Qin et al. 2025).

Notwithstanding its late ending, there have also been indications of an early start to reionisation. Recent re-analyses of the cosmic microwave background (CMB) revealed that this could relieve tensions between baryonic acoustic oscillation and CMB measurements (Sailer et al. 2026; Bera et al. 2025; though other tensions may arise as a result, cf. Cain et al. 2025). Deeper into the heart of the reionisation era when quasars become exceedingly rare, the steadily declining Ly α emission strength observed

in galaxy spectra can instead be used as a robust, independent probe of an increasingly neutral IGM (Neyer et al. 2025). While statistical analyses of recent JWST observations up to $z \approx 14$ infer a steady increase with redshift in the global neutral hydrogen fraction (Tang et al. 2024c; Jones et al. 2024; Kageura et al. 2025), Ly α emitting galaxies (LAEs) have long been known to exist even at $z > 7$ (e.g. Ono et al. 2012; Finkelstein et al. 2013; Oesch et al. 2015; Zitrin et al. 2015; Roberts-Borsani et al. 2016; Larson et al. 2022; Tang et al. 2023; Endsley & Stark 2022; Cooper et al. 2024; Leonova et al. 2025).

Despite the substantial Ly α scattering cross section expected from a predominantly neutral IGM, several of these LAEs exhibit surprisingly high equivalent width (EW) emission arising near resonance (up to several 100 Å in the rest frame; e.g. Saxena et al. 2023, 2024a; Tang et al. 2024a,b; Willott et al. 2025; Navarro-Carrera et al. 2025; Napolitano et al. 2025). Even if the bulk of the IGM is still neutral, these galaxies are expected to be located in rare ionised oases or ‘bubbles’ with sizes of the order of 1 physical Mpc (pMpc; Witstok et al. 2024, 2025b; Runnholm et al. 2025; Chen et al. 2025; Martin et al. 2026), at times challenging theoretical predictions (e.g. Lu et al. 2024; Neyer et al. 2024). On the other hand, there is mounting evidence for strong damped Ly α (DLA) absorption ($N_{H I} > 10^{22}$ cm $^{-2}$; Heintz et al. 2024, 2025a,b; Hainline et al. 2024a; D'Eugenio et al. 2024; Pollock et al. 2026), which suggests the presence of large, neutral gas reservoirs surrounding galaxies in their early assembly stages, potentially inhibiting the escape of Lyman-continuum (LyC) radiation. While the presence of Ly α emitting galaxies (LAEs) at $z > 8$ suggest that at least a small

arXiv:2603.18775v1 [astro-ph.GA] 19 Mar 2026

fraction of the Universe was already ionised, it remains unclear how common such early bubbles are, and when they first formed.

From the JWST Advanced Deep Extragalactic Survey (JADES; Eisenstein et al. 2026), a major surprise came with the discovery of exceptionally strong Ly α emission in JADES-GS-z13-1-LA (GS-z13-1-LA for short) at $z \approx 13$, which exhibited a rest-frame EW of at least 43 Å (Witstok et al. 2025a; W25 hereafter). Although seemingly at odds with the emerging late reionisation paradigm, conventional reionisation models are able to accommodate such an early LAE: Qin & Wyithe (2025) predicted a Ly α transmission of $\sim 13\%$ and estimated a probability of up to 10% of observing similarly strong Ly α emission as seen in GS-z13-1-LA. In Cohon et al. (2025), it was estimated that the observed Ly α properties of GS-z13-1-LA imply the global neutral fraction of the Universe at $z = 13$ should be $x_{\text{H I}} \lesssim 95\%$, and that there is a non-negligible probability for this source to host an active galactic nucleus (AGN).

Based on Near-Infrared Camera (NIRCam; Rieke et al. 2023a) imaging in the JADES Origins Field (JOF) programme (Eisenstein et al. 2025), GS-z13-1-LA was selected as the most robust candidate among the $z \gtrsim 11$ sample identified by Robertson et al. (2024), where it appeared as a very blue, spatially compact $z \approx 13$ galaxy. Spectroscopy from the Near-Infrared Spectrograph (NIRSpec; Jakobsen et al. 2022) subsequently uncovered the luminous Ly α line in addition to confirming its very steep UV slope ($\beta_{\text{UV}} \approx -3$; W25), the latter uncommon but not unique among the reionisation-era galaxy population (Cullen et al. 2023, 2024; Topping et al. 2024; Saxena et al. 2024b; Austin et al. 2025; Yanagisawa et al. 2025; Baker et al. 2025a; Jecmen et al. 2026; Marques-Chaves et al. 2026). Simultaneously, it revealed a smooth Ly α break that could be consistent with a dominant two-photon (2γ) emission (Cameron et al. 2024), although a nebular-dominated continuum appears difficult to reconcile with the blue continuum (Katz et al. 2025). Alternatively, the turnover of the continuum towards Ly α may be explained by a strong DLA absorption system ($N_{\text{H I}} \approx 10^{22.8} \text{ cm}^{-2}$; W25). Effectively unresolved in NIRCam imaging, W25 conservatively estimated its half-light radius in the rest-frame UV to be $r \lesssim 35 \text{ pc}$.

Despite the 18.7 h depth of the initial NIRSpec data set presented in W25, the intrinsic faintness of GS-z13-1-LA called for confirmation and more precise characterisation of the remarkable physical properties inferred from the continuum shape and Ly α line emission. Improved signal-to-noise ratio (SNR) could elucidate the origin of the continuum turnover and reveal other rest-frame UV lines to pin down the systemic redshift, thus shining light on the remarkable efficiency of ionising photon production and escape in GS-z13-1-LA as implied by the Ly α emission. In this work, we present new NIRSpec observations consisting of a 3 \times deeper exposure in NIRSpec/PRISM obtained as part of the Observing All phases of Stochastic Star formation (OASIS) Cycle-2 JWST programme (ID 5997, PIs: T. Looser & F. D’Eugenio; Looser et al. in prep.).

The outline of this work is as follows. In Section 2, we discuss the observations underlying this work. Our results are presented in Section 3 and discussed in Section 4, with Section 5 providing a summary. We adopt a flat Λ CDM cosmology throughout, with $H_0 = 67.4 \text{ km s}^{-1} \text{ Mpc}^{-1}$, $\Omega_{\text{m}} = 0.315$, $\Omega_{\text{b}} = 0.0492$ based on the latest results of the Planck collaboration (Planck Collaboration et al. 2020). On-sky separations of 1'' and 1' correspond to 3.53 physical kpc (pkpc) and 0.212 pMpc, respectively. Magnitudes are in the AB system (Oke & Gunn 1983), emission-line wavelengths in vacuum, and EWs in the rest frame.

2. Observations

2.1. JWST observing programmes

The NIRCam and NIRSpec observations of GS-z13-1-LA presented in Robertson et al. (2024) and W25, respectively, are associated with JWST guaranteed time observations (GTO) programme IDs (PIDs) 1180 (PI: D. Eisenstein), 1210, and 1287 (PI: N. Lützgendorf), and with the JOF general observer (GO) programme (PID 3215, PIs: D. Eisenstein & R. Maiolino; Eisenstein et al. 2025). Details on the JADES survey strategy and data reduction can be found in the survey overview (Eisenstein et al. 2026) and data release (DR¹) papers for NIRCam (Rieke et al. 2023b; Johnson et al. 2026; Robertson et al. 2026) and/or NIRSpec (Bunker et al. 2024; D’Eugenio et al. 2025a; Curtis-Lake et al. 2025; Scholtz et al. 2025). Within JADES, GS-z13-1-LA is associated with NIRCam ID 13731 and NIRSpec ID 20013731.

The NIRSpec observations presented in W25 consisted of 18.7 h in the low-resolution PRISM/CLEAR mode ($R \approx 100$; ‘PRISM’ hereafter) and 4.7 h in the medium-resolution G235M/F170LP grating-filter combination ($R \approx 1000$). They were obtained between 10 and 11 January 2024 as part of the DEEP/JWST tier in JADES (PID 1287; see e.g. Scholtz et al. 2025 for more details on the survey tiers). In this work, we combine these data with the successful repetition of one of three visits that originally failed due to the loss of the guide-star lock (see also Carniani et al. 2024), which adds 9.3 h in the PRISM and 2.3 h in G235M. Additionally, we make use of the 28 h NIRSpec/PRISM measurements obtained as part of OASIS between 6 and 7 January 2025, in which GS-z13-1-LA was placed on the micro-shutter array (MSA; Ferruit et al. 2022) as a supplementary, high-value target. These observations were taken with the same exposure sequence as in PID 1287, though with a different MSA configuration and hence intra-shutter position, as shown in Fig. 1. New total exposure times are summarised in Table 1.

Finally, we revisit the medium-resolution NIRSpec G235M/F170LP observations from PID 1287, which in W25 only comprised 4.7 h due to the same guide-star lock failure, but are now completed to 6.9 h depth as initially scheduled. Furthermore, they are complemented with another 9.3 h of G235M data from a pilot NIRSpec dense-shutter spectroscopy (DSS) survey, obtained as part of rescheduled observations from the JOF programme (D’Eugenio et al. 2025b). However, due to the 30% reduced line-flux sensitivity of the DSS observing strategy², the effective exposure time for the DSS observations is $0.7^2 \times 9.3 \text{ h} \approx 4.6 \text{ h}$. Altogether, this results in an expected $\sqrt{(6.9 \text{ h} + 4.6 \text{ h})/4.7 \text{ h}} \approx 1.56\times$ increase in sensitivity with respect to W25.

2.2. JWST/NIRSpec data reduction

For all available NIRSpec spectroscopy, we used the NIRSpec GTO Collaboration data reduction pipeline v5.1, as described in DR4 paper II (Scholtz et al. 2025). Compared to the previous v3 pipeline adopted in DR3 (D’Eugenio et al. 2025a) and the results presented in W25, the main changes are to adopt more recent NIRSpec calibration files and to include improved wavelength and

¹ JADES high-level science products are made publicly available at <https://archive.stsci.edu/hlsp/jades> (NIRCam DRs) as well as at <https://jades.herts.ac.uk/> (NIRSpec DR4).

² This is a result of the marginally higher background level, which is counteracted in terms of survey speed by a 4-5 \times increase in target density (cf. D’Eugenio et al. 2025b).

flux calibration corrections depending on intra-shutter offsets. Given the spatial compactness of GS-z13-1-LA (Robertson et al. 2024), we default to one-dimensional spectra extracted from a 3-pixel aperture to optimise the SNR. As in the Supplementary information of W25, however, we have verified that our findings on the spectral shape and normalisation are robust against changing to the standard full (5-pixel) aperture. This also holds for the line emission, including in a reduction where only the two outer nod positions are considered (instead of the default three, which may cause self-subtraction if the emission extends beyond the central micro-shutter; Section A). For the PRISM spectroscopy, a total of 144 sub-exposures from PIDs 1287 and 5997 (72 each) are available with a total exposure time of 56 h (Table 1). These one-dimensional sub-exposures were filtered and combined using the prescription described in Hainline et al. (2024a), W25, and Witstok et al. (2026), as part of which we also constructed the covariance matrix in a bootstrapping procedure with 5000 iterations.

We performed this combination process with all 144 PRISM sub-exposures to obtain a final, one-dimensional spectrum. Using the same procedure, we additionally created combined spectra after having split up the dataset into the 72 sub-exposures taken as part of PID 1287 (JADES) and 5997 (OASIS). A comparison of these separate JADES and OASIS spectra will be discussed further in Section 3.1, especially in light of the different intra-shutter positions between these two observations, both near the edge of one of NIRSpec’s micro-shutters, but critically at almost opposite ends along the dispersion direction (Fig. 1a).

3. Results

3.1. Comparison of JADES and OASIS observations

3.1.1. A first look at the continuum properties

The resulting one-dimensional NIRSpec/PRISM spectra from the JADES and OASIS observations are shown in Fig. 1b. From this comparison it becomes clear that, especially considering the estimated uncertainties, the new OASIS data show excellent agreement with the spectrum based on (the initial 67% of) the JADES observations previously reported in W25. Both the now complete JADES spectrum and the new OASIS spectrum confirm the overall continuum shape with a clear spectral break at $\lambda_{\text{obs}} \approx 1.7 \mu\text{m}$, as well as its normalisation.

More specifically, we have verified that synthetic NIRSpec photometry in both the OASIS and JADES spectroscopy continues to agree well with NIRCам photometry. Indeed, with the updated NIRSpec calibration files (Section 2.2) the agreement is slightly improved compared to what was found in W25, though we still find the NIRSpec synthetic photometry to be systematically lower, by approximately 20%. As before, this small residual difference does not display a clear trend with wavelength, and this is within the level of systematic uncertainty expected from the finite pointing accuracy and substantial gradient in slit losses near the edge of the micro-shutter³, where GS-z13-1-LA is observed (see Fig. 1a). Unless mentioned otherwise, we therefore apply a minor additional path-loss correction to both spectra in the following, updated to the new spectroscopic measurements but otherwise using the same routine as described in W25. We use the NIRCам photometry obtained by forcepho (B. D. Johnson et al. in prep.; see also e.g. Robertson et al. 2023; Tacchella et al.

³ The MSA pointing accuracy is ~ 20 mas, which at the edge of the micro-shutter translates into transmission differences of $\gtrsim 10\%$ (Ferruit et al. 2022).

Table 1. Summary of NIRSpec observations of GS-z13-1-LA as part of the JADES, JOF, and OASIS programmes (Section 2.1).

	JADES	OASIS	JOF	Combined
PID	1287	5997	3215	–
$t_{\text{exp, PRISM}}$ (h)	28	28	–	56
$t_{\text{exp, G235M}}$ (h)	6.9	–	9.3*	16.2*
F_{19}	6.3 ± 1.0	7.9 ± 1.2	–	7.1 ± 0.8
SNR	6.1	6.4	–	8.8

Notes. Listed properties are programme ID (PID), exposure time (t_{exp}) in the PRISM and G235M, and simple estimates from the PRISM spectra of the line flux in units of $10^{-19} \text{ erg s}^{-1} \text{ cm}^{-2}$ (F_{19}) and SNR.

(*) With (partially) increased background noise level (see text for details).

2023; Baker et al. 2025b), noting that the regular aperture photometry yields consistent results.

3.1.2. Initial Ly α line measurements

Crucially, the NIRSpec/PRISM observations from OASIS also reaffirm the bright emission line. More quantitatively, we confirm that the emission line fluxes seen in the JADES and OASIS data agree within uncertainties, as summarised in Table 1. We obtained line fluxes by direct integration after path-loss correction and continuum subtraction⁴, having selected 7 wavelength bins where the combined spectrum reaches $\text{SNR} > 3$ for ease of comparison (grey shading in Fig. 1b; more sophisticated estimates will be provided in Section 3.2). Moreover, we find that the integrated difference between the two spectra across the same wavelength bins is statistically consistent with zero, $\Delta F = (1.35 \pm 1.32) \times 10^{-19} \text{ erg s}^{-1} \text{ cm}^{-2}$.

While the line was already significantly detected by W25 in the initial 18.7 h, a particularly encouraging trend emerges from the integrated line SNRs. The initial W25 dataset shows $\text{SNR} \approx 5$ (re-measured here with consistent continuum-subtraction method), which is seen to increase from $\text{SNR} \approx 6$ in both the complete JADES and OASIS spectra (28 h each), and finally $\text{SNR} \approx 9$ for the combined 56 h of observations. The scaling is in lockstep with the square root of the exposure time, precisely as expected for a real signal.

We recall that, as discussed in W25, the observed discontinuity at $1.7 \mu\text{m}$ —more than 3 mag between the NIRCам F150W and F200W filters—leaves no other credible alternative than for the redshift to be $z \approx 13$, and hence for the line to be Ly α . Furthermore, line emission from a low-redshift interloper (e.g. H α at $z \approx 1.60$, [O III] λ 5008 Å at $z \approx 2.41$, or [O II] λ 3727, 3730 Å at $z \approx 3.58$) would require both an unprecedented EW (observed $\text{EW} \gtrsim 10\,000$ Å) as well as unphysical line ratios to explain the absence of other strong lines (e.g. Pa α , H β , and [O III]) that are expected to be present for all of these redshift solutions.

Having confirmed the line in the new PRISM observations, we considered the deeper NIRSpec/G235M data, consisting of a 9.3 h exposure from the DSS survey presented in D’Eugenio et al. (2025b) and the now fully completed 6.9 h obtained as part of JADES (Section 2.1). Encouragingly, compared to medium-resolution G235M observations considered in W25, a small flux excess does indeed appear within a spectral aperture of $\Delta\nu \approx 1000 \text{ km s}^{-1}$ centred on $\lambda_{\text{obs}} = 1.7171 \mu\text{m}$ (the central

⁴ Based on the best-fit continuum obtained from the full spectral modelling in Section 3.2.

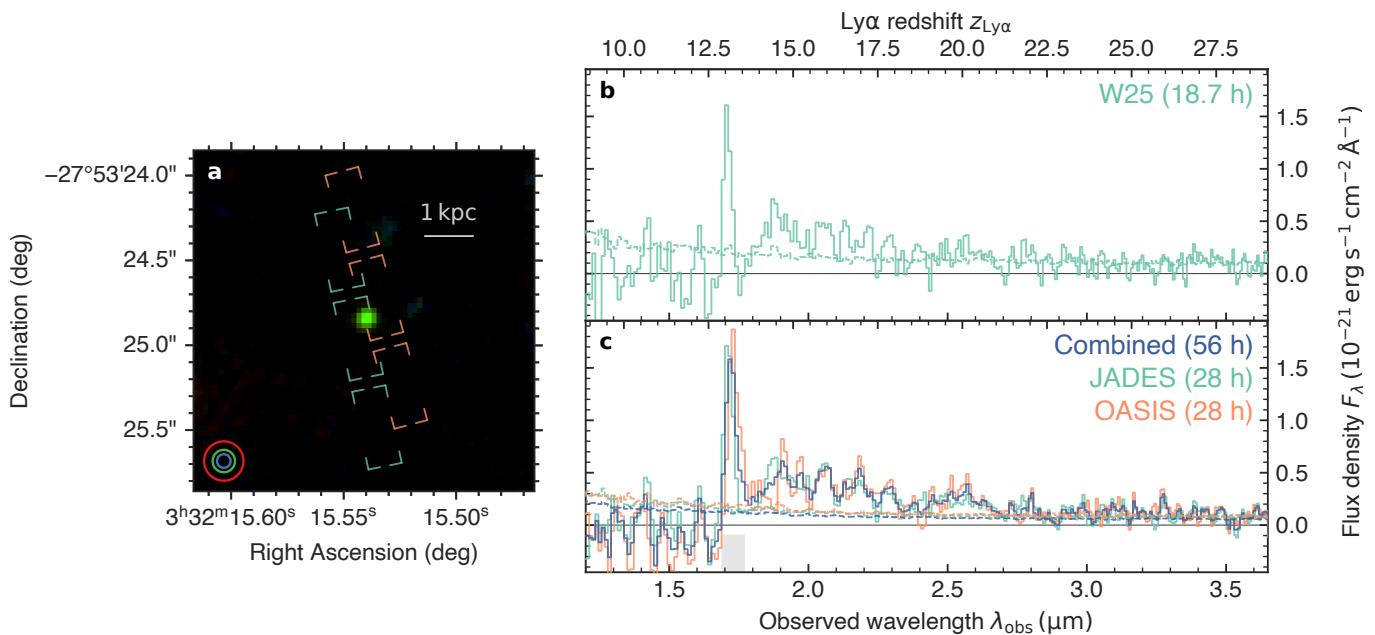


Fig. 1. NIRCam and NIRSpec/PRISM observations of GS-z13-1-LA. **a**, False-colour NIRCam image with the F090W, F115W, F150W, and F162M filters shown as blue, F182M, F200W, F210M, F250M, and F277W as green, and F300M, F335M, F356W, F410M, F444W, and F480M as red (stacked at native resolution). For reference, the point spread function FWHM of the F115W, F200W, and F356W filters are shown in the bottom-left corner. The triplet of NIRSpec micro-shutters that were opened in the JADES and OASIS observations are shown in teal and orange, respectively. A physical scale of 1 kpc at $z = 13$ is indicated by the horizontal white line. **b**, One-dimensional NIRSpec/PRISM spectrum from JADES (W25). **c**, PRISM spectra from the completed JADES (teal) and new OASIS (orange) observations, and the combined spectrum (dark blue). The grey shading indicates the wavelength range over which the Ly α line fluxes are integrated (Table 1). 1σ uncertainty on individual wavelength bins is shown by dashed lines in panels b and c.

wavelength inferred from the PRISM spectra; Section 3.2.2). While the excess is still decidedly marginal (just over 1σ), we have verified that this is in line with expectations based on the PRISM flux measurements, if the line is spectrally resolved in the $R \approx 1000$ observations (Section A).

An upcoming Cycle-4 programme (PID 9016, PI: D. Stark) will target GS-z13-1-LA, among other notable galaxies around GOODS-S, using G235M/F170LP for an additional 45 h, nearly quintupling the total exposure time. Provided the intrinsic line full-width at half maximum is not too large ($\text{FWHM} \lesssim 1000 \text{ km s}^{-1}$), our current sensitivity levels (Section A) suggest that this should provide sufficient depth for a more robust detection of the line and shed light on its width.

Closer examination of the spectral shape of the line observed in the PRISM observations reveals that its peak appears ever so slightly offset between the two separate spectra, of the order of a single wavelength bin. We deem it unlikely to be a real physical effect due to intrinsic time variability, given the relatively short delay in the rest frame of approximately one month between the JADES and OASIS observations. Another physical explanation is that the Ly α emission, contrary to the UV continuum, could be spatially extended (as observed in e.g. GN-z11 at $z = 10.6$; Bunker et al. 2023; Scholtz et al. 2024), possibly causing the two different micro-shutter placements to trace distinct sub-regions where the line exhibits different peak velocity offsets (e.g. Leclercq et al. 2020). However, we do not see evidence for spatially extended emission in the two-dimensional spectra (Section A), and the implied velocity difference still appears unrealistically large, since the observed wavelength of the line coincides with the lowest spectral resolution of the PRISM (where individual bins have a velocity width of $\Delta v \approx 2000 \text{ km s}^{-1}$; Jakobsen et al. 2022). We instead attribute this to a combina-

tion of relatively modest SNR and the changing intra-shutter positions of GS-z13-1-LA, which were nearly at opposite ends of the NIRSpec micro-shutter between the two programmes, for reasons discussed in more detail below.

Wavelength offsets in NIRSpec/PRISM at the level of $\Delta v \sim 1000 \text{ km s}^{-1}$ have been reported previously in sources where accurate redshift measurements are available from the higher-resolution gratings ($R \approx 1000$; e.g. Bunker et al. 2024; de Graaff et al. 2025). Based on JADES DR3 data, D’Eugenio et al. (2025a) demonstrated that an exceptionally clear correlation ($p < 10^{-30}$) exists between these offsets and the intra-shutter position of sources along the dispersion direction. As such, the effect can be interpreted as small imperfections of the NIRSpec wavelength solution for sources that are offset from the micro-shutter centre. While the standard NIRSpec data reduction algorithms⁵ already include a zero-point wavelength refinement as a function of intra-shutter source displacement, until recently this calibration was entirely based on pre-flight instrument models (Alves de Oliveira et al. 2018; Ferruit et al. 2022).

Steadily growing datasets, however, have prompted efforts to empirically calibrate any remaining inaccuracies, including within JADES DR4 (Scholtz et al. 2025). However, the blue wavelength range of NIRSpec ($\lambda_{\text{obs}} \lesssim 2 \mu\text{m}$) poses the most difficult regime to perform this correction, since this requires a large number of emission lines detected at high SNR, ideally from sources that remain (close to being) spatially unresolved.

⁵ These algorithms are shared between the standard Space Telescope Science Institute (STScI; <https://jwst-docs.stsci.edu/jwst-science-calibration-pipeline>) and the NIRSpec GTO data reduction pipelines (Section 2.2 and Scholtz et al. 2025).

Although strong optical lines (e.g. [O III] λ 4960, 5008 Å, H β , H α) can be readily observed in galaxies at $z \lesssim 3$, the JADES target selection was designed to favour higher-redshift sources (Bunker et al. 2024; Curtis-Lake et al. 2025), resulting in reduced number statistics below $\sim 2 \mu\text{m}$ available for this analysis (Fig. 5 in Scholtz et al. 2025). Furthermore, these lower-redshift sources are typically spatially extended, thus likely hindering an accurate empirical determination of the wavelength zero-point calibration for a given intra-shutter position.

Statistically speaking, the empirically calibrated routine implemented within the v5.1 NIRSpec GTO pipeline yields a clear improvement to the PRISM wavelength offsets, as shown in Fig. 4 of Scholtz et al. (2025). Due to the limited statistics at $\lambda_{\text{obs}} \lesssim 2 \mu\text{m}$, however, minor discrepancies of the order of $\sim 1000 \text{ km s}^{-1}$ remain in individual sources, as is also the case in the peak Ly α wavelength between the OASIS and JADES observations (Fig. 1). Recalling the absence of significant differences in the Ly α emission between different spectral extraction apertures (Section 2.2), which suggests that the line emission is likely spatially compact, we conclude that remaining calibration systematics could reasonably cause the observed wavelength shift. In the following section, we therefore turn to the Bayesian spectral fitting method presented in W25 to marginalise over the remaining wavelength discrepancy between the JADES and OASIS observations.

3.2. Spectral line and continuum modelling

3.2.1. Model set-up

To reassess the line and continuum properties of GS-z13-1-LA from the full 56 h of observations, we repeated the spectral modelling presented in W25.⁶ We refer to the Methods section of that work for further details, before briefly summarising the model setup and outlining minor changes below. When comparing model variants to each other, we will explicitly define an *italicised shorthand* for each variant.

The fitting routine aims to reproduce the observed Ly α and continuum emission within the observed wavelength range $1.6 \mu\text{m}$ to $2.9 \mu\text{m}$ (where the continuum is detected at $\text{SNR} \gtrsim 1$ per wavelength bin). The model takes into account instrumental effects in the form of the NIRSpec/PRISM line spread function⁷, while physical effects include the Ly α damping-wing absorption from intervening neutral hydrogen in the IGM, which is assumed to be neutral except for a potential ionised bubble, as well as from potential proximate DLA systems. Ionising photons, whose rate is parametrised by the production efficiency ξ_{ion} , contribute to Ly α visibility either through (i) direct conversion into Ly α photons via recombinations, or (ii) indirect Ly α transmission enhancement via ionised bubble growth. The relative importance of these two processes is modulated by the LyC escape fraction of the galaxy, $f_{\text{esc, LyC}}$ (in the default *single-source* model). In addition, we considered a more agnostic approach here where we simply vary the ionised bubble radius with a log-uniform prior, $\log_{10} R_{\text{ion}} \text{ (pMpc)} \sim \mathcal{U}(-2, 0)$ (the upper bound of 1 pMpc being motivated by simulation predictions at a neutral fraction of $x_{\text{H I}} \gtrsim 80\%$; Lu et al. 2024; Neyer et al. 2024), without requiring any LyC leakage from GS-z13-1-LA itself (*collective* model).

We adopted the same (log-)uniform prior distributions on our fitting parameters as in W25 except for the systemic red-

Table 2. Spectral line and continuum modelling results.

Parameter	(Logarithmic) units	Value
z_{sys}		$13.07^{+0.04}_{-0.02}$
C	$10^{-21} \text{ erg s}^{-1} \text{ cm}^{-2} \text{ \AA}^{-1}$	$0.25^{+0.03}_{-0.03}$
β_{UV}		$< -3.27 (3\sigma)$
R_{ion}	pMpc	$0.167^{+0.070}_{-0.062}$
$\log_{10}(\xi_{\text{ion}})$	Hz erg^{-1}	$26.43^{+0.30}_{-0.15}$
$f_{\text{esc, LyC}}$		$0.55^{+0.25}_{-0.29}$
$F_{\text{Ly}\alpha}$	$10^{-19} \text{ erg s}^{-1} \text{ cm}^{-2}$	$6.6^{+0.5}_{-0.5}$
$L_{\text{Ly}\alpha}$	$10^{43} \text{ erg s}^{-1}$	$1.1^{+0.2}_{-0.2}$
$\text{EW}_{\text{Ly}\alpha, \text{pre-IGM}}$	Å	431^{+106}_{-84}
$\text{EW}_{\text{Ly}\alpha}$	Å	66^{+10}_{-9}
$f_{\text{esc, Ly}\alpha}$		$0.152^{+0.024}_{-0.020}$
$\Delta v_{\text{Ly}\alpha, \text{pre-IGM}}$	km s^{-1}	843^{+107}_{-174}
$\Delta v_{\text{Ly}\alpha}$	km s^{-1}	1164^{+686}_{-658}
$\sigma_{\text{Ly}\alpha, \text{pre-IGM}}$	km s^{-1}	448^{+77}_{-85}
Δp_0	bins	$0.55^{+0.36}_{-0.29}$
Δp_1	bins	$-0.62^{+0.33}_{-0.33}$
χ^2_{ν}		1.22
BIC		350

Notes. Reported model parameters are the systemic redshift (z_{sys}), normalisation (C) and slope (β_{UV}) of the power-law continuum, LyC production efficiency (ξ_{ion}) and escape fraction ($f_{\text{esc, LyC}}$), the Ly α peak velocity offset ($\Delta v_{\text{Ly}\alpha, \text{pre-IGM}}$) and velocity dispersion ($\sigma_{\text{Ly}\alpha, \text{pre-IGM}}$) before IGM transmission (i.e. as the line profile emerges from the galaxy), and the two wavelength corrections Δp_i . Additionally, we report the χ^2_{ν} and BIC values, as well as the following quantities not freely varied but derived from the main parameters (see Section 3.2 and W25): the ionised bubble radius (R_{ion}), observed Ly α flux ($F_{\text{Ly}\alpha}$), intrinsic Ly α luminosity ($L_{\text{Ly}\alpha}$), the EW of Ly α before IGM transmission ($\text{EW}_{\text{Ly}\alpha, \text{pre-IGM}}$) and afterwards (as observed; $\text{EW}_{\text{Ly}\alpha}$), the escape fraction of Ly α ($f_{\text{esc, Ly}\alpha}$), and the observed Ly α velocity offset ($\Delta v_{\text{Ly}\alpha}$).

shift, here slightly expanded to $z_{\text{sys}} \sim \mathcal{U}(12.7, 13.5)$. In addition, the prior on the Ly α velocity offset (before encountering the neutral IGM) was previously assumed to follow $\Delta v_{\text{Ly}\alpha, \text{pre-IGM}} \sim \mathcal{U}(0, 500) \text{ km s}^{-1}$, but we conservatively extend its upper bound here to 1000 km s^{-1} . Based on the absolute UV magnitude of GS-z13-1-LA ($M_{\text{UV}} \approx -18.5 \text{ mag}$; W25), such a high Ly α velocity offset would be unlikely, but perhaps not entirely unfeasible, when compared to observations ranging from $z \sim 2$ (Erb et al. 2014; Steidel et al. 2014) to $z \sim 11$ (see e.g. Mason et al. 2018; Qin & Wyithe 2025 for literature compilations). Observational evidence has moreover long suggested that, especially at $z \gtrsim 5$, Ly α line profiles could have prominent non-Gaussian scattering wings, which may extend out to several hundreds of km s^{-1} redwards of line centre (Bunker et al. 2003; Erb et al. 2014; Smit et al. 2017; Pentericci et al. 2018; Hayes et al. 2021; Witstok et al. 2021; Tang et al. 2024a; Yuan et al. 2025; Prieto-Lyon et al. 2025). The main effect of this extended prior range is a larger uncertainty on the inferred systemic redshift, which remains unclear despite the 56 h depth of the complete JADES and OASIS observations, as discussed further below.

⁶ Code available at https://github.com/joriswitstok/lymana_absorption.

⁷ Based on the resolution curve in the STScI documentation, enhanced by $1.5\times$ to match the Ly α line width in the PRISM as described in W25.

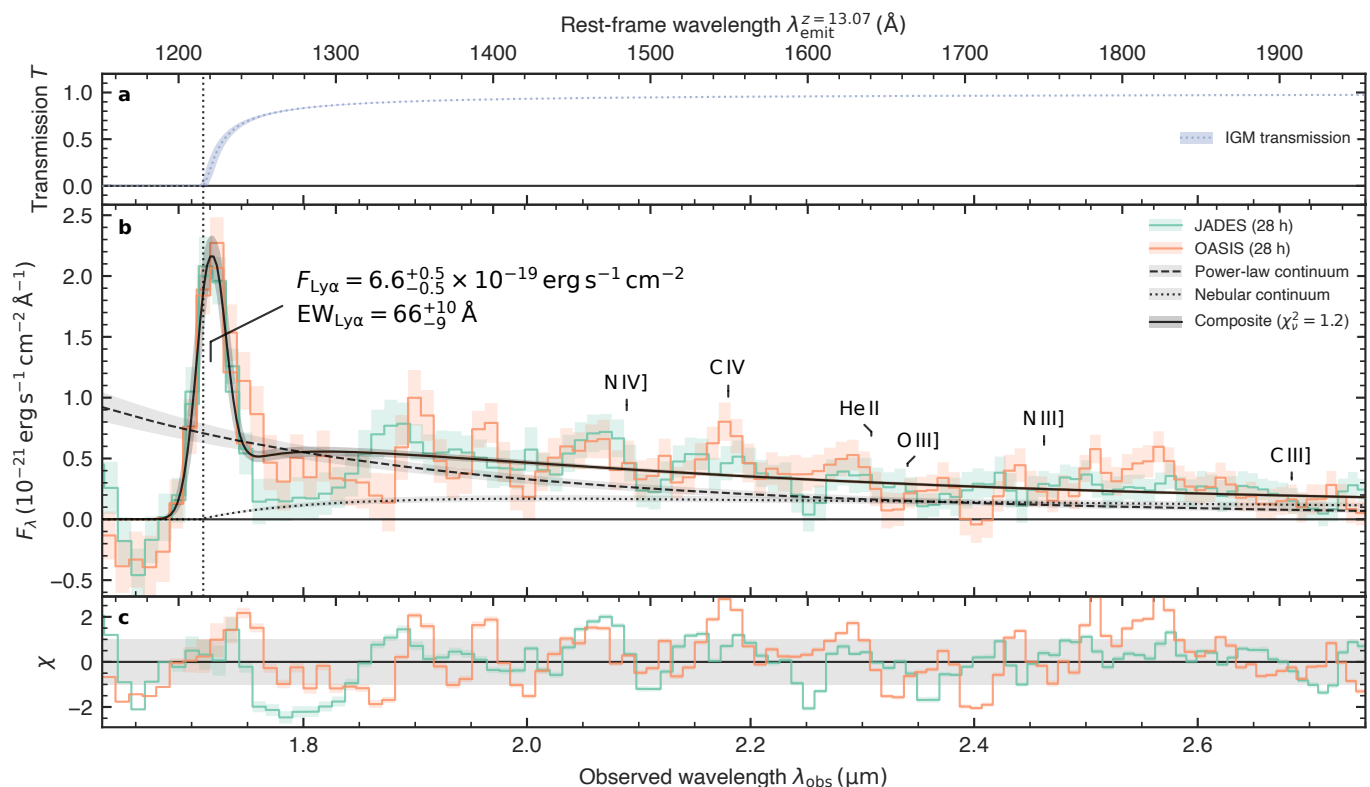


Fig. 2. Modelled NIRSpec/PRISM observations of GS-z13-1-LA. **a**, Model curves for the IGM transmission T , according to the legend on the right. **b**, Coloured lines show the path-loss corrected PRISM spectra observed in JADES and OASIS (Section 2.1). The best-fit model spectrum is shown by the black solid line, while its individual power-law and nebular-continuum components are shown with dashed and dotted lines, respectively. The observed Ly α flux and EW in the best-fit model are annotated. The expected location of rest-frame UV lines is indicated for the model’s best-fit systemic redshift of $z = 13.07$, although we note that none are confidently detected (Section 4). **c**, Uncertainty-normalised residuals χ are shown for the two different spectra.

Following Hviding et al. (2025), as a means of refined wavelength correction we applied a constant shift of Δp_i in units of wavelength bins, treating the JADES ($i = 0$) and OASIS ($i = 1$) spectra separately. This results in an absolute wavelength correction most notable around $\lambda_{\text{obs}} \approx 1.6 \mu\text{m}$, where the spectral resolution of the NIRSpec/PRISM is lowest.⁸ We adopted a Gaussian prior with $\mu_{\Delta p_i} = 0$ and $\sigma_{\Delta p_i} = 0.5$, truncated at $|\Delta p_i| = 2$.

3.2.2. Insights and results

As in W25, we considered various combinations of a power law and/or a nebular continuum as the underlying continuum emission: a *pure power-law* continuum, a *pure two-photon* continuum, and a *composite* model with a power-law and nebular continuum. To reproduce the continuum downturn near Ly α , we explored models where the power-law continuum is affected by DLA absorption (*IGM and DLA*) in addition to the fiducial *pure IGM* absorption model. However, noting that the turnover near Ly α is less pronounced in the new OASIS spectrum compared to JADES—that is, it does not tend to zero at the Ly α wavelength to the same degree—we tested the introduction of a covering fraction of the DLA-absorbing gas in the *IGM and DLA* model. The associated geometry, where a central source is only par-

⁸ The reason for working in wavelength bins (whose size is tied to $1.59 \times$ the width of a native detector pixel in the NIRSpec GTO pipeline) is the wavelength-dependent spectral resolution of the PRISM, which means that they sample an irregular grid in wavelength space (Jakobsen et al. 2022; see also e.g. de Graaff et al. 2025; Scholtz et al. 2025).

tially covered by dense neutral H I gas (e.g. an edge-on disc), would also provide a natural explanation for the simultaneous, efficient escape of Ly α photons, as discussed in W25 (see also Section 4.1).

Statistically, however, based on the combined JADES+OASIS data we find that a *pure IGM* absorption model produces an equally satisfactory fit as a model with DLA absorption (*IGM and DLA*; both a reduced chi-squared value of $\chi^2_{\nu} = 1.22$). In terms of the Bayesian information criterion (BIC), the former is slightly preferred (BIC = 350 versus BIC = 360, respectively), although we note that this is mainly true with the *composite* model, whereas in the *pure power-law* model the preference becomes less strong. For simplicity, we consider the family of models without DLA absorption in what follows.

On the other hand, we confirm that a *pure two-photon* continuum continues to be disfavoured over the *pure power-law* model ($\chi^2_{\nu} = 1.37$ versus $\chi^2_{\nu} = 1.22$ and BIC = 382 versus BIC = 349, respectively), owing to the very blue continuum of GS-z13-1-LA. Otherwise, however, we see little difference statistically between power-law continuum models either with the addition of a nebular continuum (*composite*), or without it (*pure power-law*; both $\chi^2_{\nu} = 1.22$, $|\Delta\text{BIC}| < 1$). As our fiducial model, we opt here for the case where nebular continuum is included. The best-fitting results for this 9-parameter model are shown in Fig. 2 and summarised in Table 2. The full posterior distributions are presented in Section B.

The *collective* model, which does not require any LyC leakage from GS-z13-1-LA but instead simply imposes an ionised bubble

to be in place, yields virtually identical results both in terms of fit quality and (most) best-fit parameters as the *single-source* model. The exception is the ionising-photon production efficiency, which is reduced by 0.5 dex to $\log_{10} \xi_{\text{ion}} (\text{Hz erg}^{-1}) = 25.91_{-0.22}^{+0.12}$, although this comes at the expense of requiring a larger ionised bubble, $R_{\text{ion}} = 0.48_{-0.33}^{+0.24}$ pMpc. Therefore, the *collective* model carries the implicit assumption that the environment of GS-z13-1-LA has managed to ionise a significant portion of the surrounding IGM. Whether or not this is a realistic scenario will be further explored in Section 4.2.

We recall that the normalisation of the nebular continuum is self-consistently coupled to the Ly α luminosity, which itself is controlled by ξ_{ion} (and $f_{\text{esc, LyC}}$ in the *single-source* ionised bubble model). We computed nebular continuum templates with the `PYNEB` code (Luridiana et al. 2015) under the assumption of $T = 20\,000$ K and $n = 100 \text{ cm}^{-3}$, noting that the shape of the 2γ component—which dominates at the wavelength regime considered here—is fixed (Spitzer & Greenstein 1951). The inclusion of the nebular continuum effectively acts to redden the power-law continuum, which motivates the choice for this relatively low density here as effectively the bluest UV slope, though this will be explored further in Section 4.1. As a consequence, even though the effective UV slope (power-law and nebular continuum combined) is $\beta_{\text{UV}} = -3.03$, the intrinsic UV slope is preferred to be extremely steep, $\beta_{\text{UV}} < -3.27$ (3σ). The pure power-law model, meanwhile, yields a very blue value still, $\beta_{\text{UV}} = -3.21 \pm 0.28$. We have verified that this measurement is consistent within uncertainties compared to variations of fitting the 3-pixel versus 5-pixel spectral extraction (Section 2.2), (not) including DLA absorption, and/or extending the wavelength range considered.

We find the resulting systemic redshift to be marginally higher than in W25 as a result of the improved NIRSspec wavelength solution, which differs from previous results both in terms of the NIRSspec calibration files (Section 2.2) and the additional empirical zero-point correction (Section 3.1.2). This can be traced back most directly by the observed Ly α wavelength, here inferred to be $\lambda_{\text{obs}} = 1.7171_{-0.0037}^{+0.0040} \mu\text{m}$, compared to $\lambda_{\text{obs}} = 1.7084 \pm 0.0014 \mu\text{m}$ before. The same comparison also illustrates that the introduction of Δp_i as a refined wavelength correction (Section 3.2.1) ensures that the systematic uncertainty of the wavelength solution is propagated into uncertainty estimates on all other quantities. Though degeneracy naturally exists between the two parameters Δp_i (see Section B), the overall correction converges reasonably well as seen by the $\sim 2\sigma$ deviations away from $\Delta p_i = 0$, as would be preferred by the prior.

Finally, we do not recover clear detections of any rest-frame UV emission lines other than Ly α . The OASIS spectrum does show a modest peak at the expected location of the C IV λ 1548, 1551 Å doublet, for which we infer a tentative 3.0σ detection of $F_{\text{CIV}} = (11.0 \pm 3.7) \times 10^{-20} \text{ erg s}^{-1} \text{ cm}^{-2}$ and $\text{EW}_{\text{CIV}} = 22.0 \pm 7.4 \text{ \AA}$. However, this signature is not confirmed in the JADES spectrum ($F_{\text{CIV}} = (2.8 \pm 3.7) \times 10^{-20} \text{ erg s}^{-1} \text{ cm}^{-2}$), nor does its implied redshift match up with other emission-line signatures. Upper limits on the EWs of rest-frame UV features remain at the 20 Å level (3σ) even in the combined 56 h JADES+OASIS PRISM spectrum.

We conclude that future spectroscopy will need to go substantially deeper to detect rest-frame UV features, which may be weakened as a result of a non-zero LyC escape fraction. Alternatively, medium-resolution spectroscopy as planned in the NIRSspec/G235M observations of JWST PID 9016 (PI: D. Stark) may be more efficient at isolating narrow rest-UV lines from the underlying continuum emission, while a complementary strategy is to pursue more luminous lines at longer wavelengths, such as

the [O III] 88 μm that will be targeted in the upcoming ALMA programme 2025.1.00147.S (PI: J. Witstok).

4. Discussion

Based on NIRC*am* imaging and the initial NIRS*pec*/PRISM spectroscopy obtained as part of JADES, W25 concluded that GS-z13-1-LA hosts a compact ($r \lesssim 35 \text{ pc}$), powerful source of ionising radiation—a dense cluster of massive stars or, as also favoured by Cohon et al. (2025), an AGN—responsible for driving the observed Ly α emission. Additionally, the efficient production and escape of LyC photons could also explain the likely presence of a modestly sized ionised bubble ($\sim 0.2 \text{ pMpc}$).⁹ In the following sections, we will revisit and revise these arguments.

4.1. The ionising source(s) and interstellar medium conditions within GS-z13-1-LA

Leveraging the completed JADES and new OASIS observations, the Ly α line itself and the very blue continuum are clearly confirmed. Meanwhile, our renewed statistical analysis indicates that the data are consistent with what is expected from a fully neutral IGM without necessitating DLA absorption. This resolves the potential issue of having to explain the superposition of DLA absorption and Ly α emission, although as discussed in W25, this phenomenon has been reported in AGN (Wu et al. 2024) and nearby star-forming galaxies (Hu et al. 2023). Moreover, in the absence of dust, the overall Ly α transmission could be aided to some degree by resonant scattering in neutral gas, whereby the Ly α photons would gain a systemic velocity offset that decreases their probability of subsequently being scattered out of the line of sight by neutral gas in the IGM.

Alternatively, it is also conceivable that the observed difference in continuum turnovers between JADES and OASIS—perhaps seen most clearly in the notable residuals of the JADES spectrum around $\lambda_{\text{obs}} \approx 1.8 \mu\text{m}$ in Fig. 2c—is real. The small NIRS*pec* micro-shutters have been shown to cause ‘pseudo-slit losses’ due to self-subtraction of spatially extended Ly α emission, although this effect is only expected to be relevant much closer to the line resonance ($\lambda_{\text{emit}} \lesssim 1250 \text{ \AA}$; Bhagwat et al. 2025), and we do not see clear evidence of self-subtraction (Section A). However, the two micro-shutter placements could preferentially probe the continuum from regions with different H I column densities, which simulations indeed predict to vary significantly between sightlines even on spatial scales of $\lesssim 100 \text{ pc}$ (Gelli et al. 2025).

In any case, the constraints on the UV continuum shape again point towards GS-z13-1-LA being a highly efficient producer of ionising radiation. Reaching a UV slope of $\beta_{\text{UV}} \approx -3$ is already challenging when the spectrum is dominated by O-type stars, the most massive and hottest stars in standard stellar models with effective surface temperatures of $T_{\text{eff}} = 40\,000 \text{ K}$ (e.g. Topping et al. 2024). Moreover, as already discussed in Section 3.2.2, the relative reddening by any nebular continuum emission requires an even bluer continuum intrinsically (see also Katz et al. 2025). This is illustrated in Fig. 3, where we compare the observed UV slope with ideal blackbody curves and nebular continua for a range of electron temperatures and densities. At least to first order, a combination of these two components is expected to give rise to the observed continuum in GS-z13-1-LA.

⁹ The scenario with an ionised bubble is strongly favoured by the non-detection in the MIRI/F770W band containing H β , since even under conservative assumptions this translates to an upper bound on the Ly α luminosity that is difficult to accommodate without a bubble (W25).

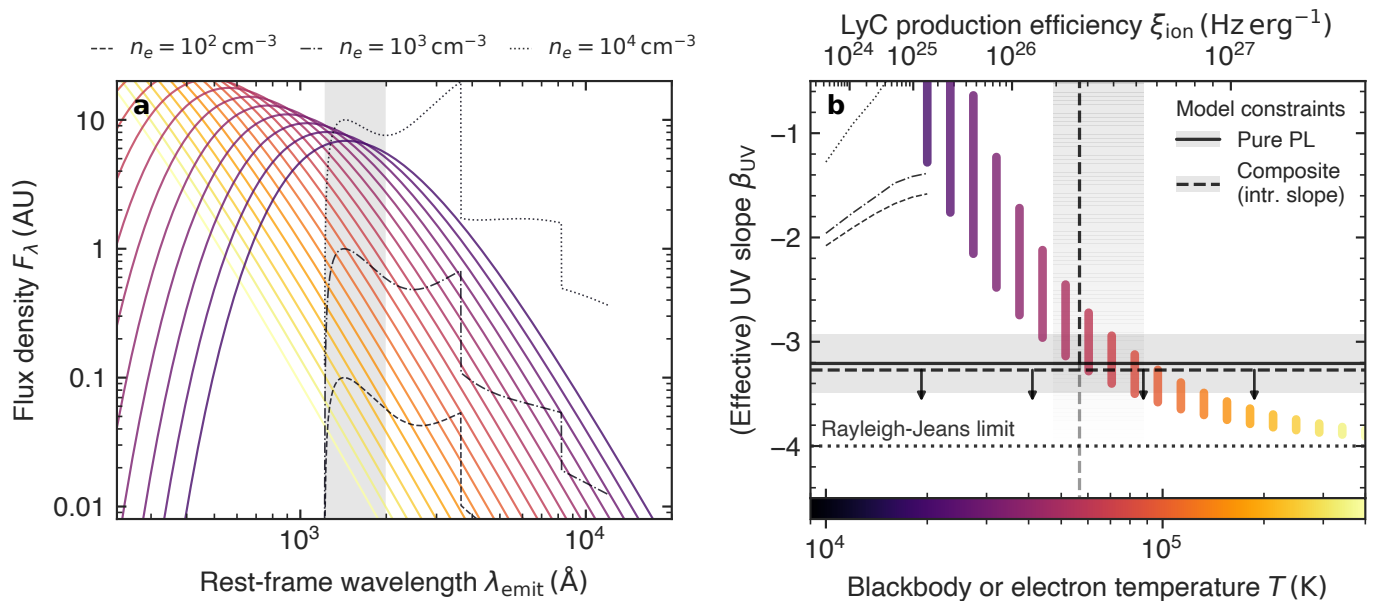


Fig. 3. **a**, Coloured lines show blackbody curves of varying temperature (according to the colourbar in panel b). Thin dashed, dash-dotted, and dotted lines show nebular continuum predictions by pyneb (Luridiana et al. 2015) for varying electron density n_e , but at fixed temperature $T_e = 10,000 \text{ K}$ (where they are bluest; cf. panel b). Grey shading indicates the approximate wavelength range probed in the spectral modelling of GS-z13-1-LA (Section 3.2.1). **b**, Effective UV slopes of blackbody spectra and nebular continua measured across the wavelength range highlighted in panel a, as a function of temperature. Thin lines show the *minimum* slope of nebular continua at different densities (according to the legend in panel a). A horizontal black line and grey shading shows the inferred UV slope of GS-z13-1-LA for a pure power-law (PL) continuum, while the horizontal dashed line indicates the upper limit obtained for the intrinsic power-law slope when including nebular continuum. Grey shading similarly indicates the inferred range on the top ξ_{ion} axis. The horizontal dotted line shows the blackbody spectral slope in the Rayleigh-Jeans limit, $F_\lambda \propto \lambda^{-4}$.

First considering the effective slope reached by pure blackbody emission, the qualitative comparison in Fig. 3b suggests that the extremely blue continuum of GS-z13-1-LA requires a source (or population of sources) reaching an (average) temperature of approximately $T \approx 50,000 \text{ K}$. The effect is magnified when a nebular continuum is present, in which case even higher temperatures of $T \geq 60,000 \text{ K}$ are required. This regime is only reached by extreme objects typically representing a small fraction of stellar populations: for instance, Wolf-Rayet (WR) stars that have shed their outer envelopes through winds or eruptions (Crowther 2007), stars stripped in binaries (e.g. Götzberg et al. 2017), or very massive stars (VMSs; Martins & Palacios 2022). Alternatively, as discussed in W25, a truncated accretion disc can reach spectral slopes steeper than $\beta_{\text{UV}} = -7/3 \approx -2.33$ (the standard thin-disc model prediction; Shakura & Sunyaev 1973). Owing to the high effective temperature, all of these sources emit a large fraction of their light beyond the hydrogen ionisation edge, which indeed fits in with the required high ξ_{ion} (Section 3.2.2). Independently, the model constraints on ξ_{ion} also translate to a blackbody temperature close to $T \approx 60,000 \text{ K}$ (Fig. 3b).

Apart from the Ly α line, the characteristics of GS-z13-1-LA bear notable resemblance to UNCOVER-37126, a galaxy at $z = 10.3$ that is also similarly spatially compact (Atek et al. 2023; Fujimoto et al. 2024). Based on its blue UV continuum measured by NIRSpec ($\beta_{\text{UV}} \approx -2.9$) and the absence of strong emission lines covered by MIRI spectroscopy (as well as ALMA observations; Algera et al. 2025), Marques-Chaves et al. (2026) recently inferred U37126 to have a near-unity LyC escape fraction. This implies an almost complete absence of the interstellar medium (ISM), attributed by Marques-Chaves et al. to extremely efficient star formation and/or strong feedback effects. While excessive gas removal and LyC escape is unlikely to be the case in GS-

z13-1-LA, precisely because of the strong Ly α emission, a brief episode of high LyC leakage in the near past could help explain the creation of the required ionised bubble. Another possibility, though not mutually exclusive, is a significant contribution from nearby galaxies to the establishment of such an ionised bubble, which will be discussed in more detail below.

4.2. The environment of GS-z13-1-LA: an early overdensity driving a large ionised bubble?

Remarkably, the one other galaxy with confirmed Ly α emission at $z > 10$, GN-z11 in the GOODS-N field (Bunker et al. 2023; Scholtz et al. 2024), was revealed to have several nearby photometric candidates consistent with its spectroscopic redshift, $z = 10.6$ (Tacchella et al. 2023). Recently, another prominent galaxy overdensity candidate at $z \approx 10.5$ in GOODS-S was reported in Wu et al. (2026). While the candidate member galaxies at this point rely on photometric selection techniques, there is tentative evidence for enhanced Ly α transmission within this structure. The analysis by Wu et al. (2026) tantalisingly reveals a radial trend in excess flux within the photometric band containing Ly α , suggesting that the Ly α transmission may be enhanced towards the centre of the overdensity. At an estimated $4\times$ enhancement in galaxy number density over the average field, this overdense region is indeed a prime candidate for hosting an early ionised bubble.

In the following, we investigate whether there is any evidence for a similar overdensity at the redshift of GS-z13-1-LA. We selected sources based on the catalogue of $z > 8$ galaxy candidates found in the GOODS-N and GOODS-S fields presented in Hainline et al. (2026), which in turn are drawn from the latest JADES NIRCcam DR5 (Johnson et al. 2026; Robertson et al.

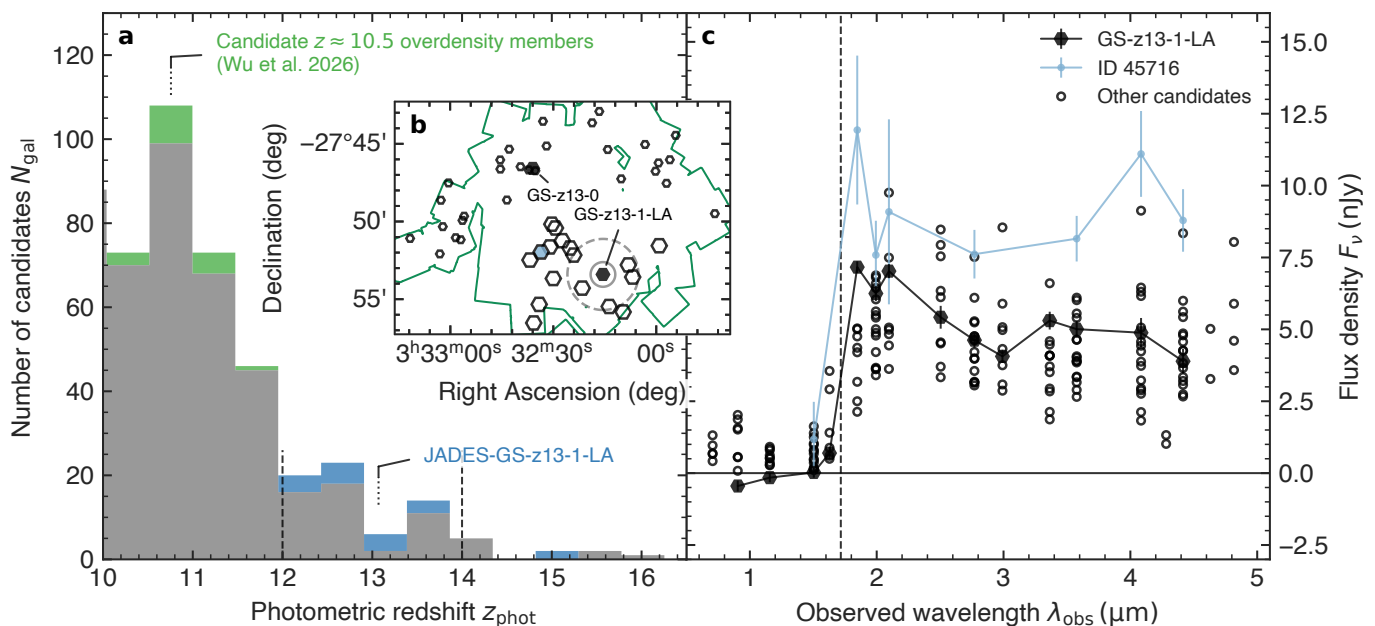


Fig. 4. **a**, Histogram of photometric redshifts from Hainline et al. (2026). Members of the candidate overdensity identified by Wu et al. (2026) are highlighted in green, those found in the vicinity of GS-z13-1-LA in blue. Two $z \approx 15$ candidates enter the selection, since accounting for DLA absorption significantly decreases their estimated redshift (see text for details). **b**, Spatial distribution of galaxy candidates found within the JADES NIRCcam footprint (solid green line; cf. Section 2.1) at $12 < z_{\text{phot}} < 14$, which are shown as small, open black hexagons. Larger hexagons mark the positions of JADES-GS-z13-0 (Robertson et al. 2023; Curtis-Lake et al. 2023; Hainline et al. 2024a), GS-z13-1-LA (both filled black and annotated), and 16 nearby galaxy candidates. The solid and dashed grey circles around GS-z13-1-LA show the projected sizes of the ionised regions in our *single-source* and *collective* model, $R_{\text{ion}} \approx 0.2$ pMpc or 0.5 pMpc, respectively (Section 3.2.2). **c**, NIRCcam photometry of GS-z13-1-LA (black hexagons) and nearby candidates (open circles). A vertical dashed line indicates the observed Ly α wavelength in GS-z13-1-LA, which falls close to the F182M medium-band filter where a tentative flux excess is seen in the brightest candidate (ID 45716, highlighted in blue).

2026). Adopting similar criteria as in Helton et al. (2024a,b) and Witstok et al. (2025b), we considered photometric redshifts obtained by Hainline et al. (2026) using eazy (Brammer et al. 2008), where we selected sources in GOODS-S at $12 < z_{\text{phot}} < 14$, a conservatively broad redshift range that will be motivated further below. We furthermore required the redshift to be relatively well-constrained, $\Delta z_1 / (1 + z) < 0.25$, where Δz_1 is the difference between the 16th and 84th percentiles of the posterior redshift distribution. Finally, we narrow down the selection to sources whose 16th (84th) percentile falls at $z > 12.8$ ($z < 13.5$), which acts to remove the spectroscopically confirmed sources JADES-GS-z12-0 at $z_{\text{spec}} = 12.48 \pm 0.01$ (ID 96216; Robertson et al. 2023; Curtis-Lake et al. 2023; D’Eugenio et al. 2024) and JADES-GS-z14-1 at $z_{\text{spec}} = 13.86^{+0.04}_{-0.05}$ (ID 18044; Carniani et al. 2024; Wu et al. 2025), respectively.

Especially at the highest redshift regime ($z \gtrsim 9$), however, photometric redshifts have regularly been found to be overestimated, at times significantly so (e.g. Fujimoto et al. 2023; Tacchella et al. 2023; Asada et al. 2025; Naidu et al. 2026; Donnan et al. 2026). This effect is, to a certain degree, expected from IGM damping-wing absorption (e.g. Keating et al. 2024a,b; Curti et al. 2025; Huberty et al. 2025; Mason et al. 2026), but in some cases has also shown to be exaggerated by extreme DLA absorption (e.g. Hainline et al. 2024a; D’Eugenio et al. 2024; Heintz et al. 2025b; Carniani et al. 2025; Pollock et al. 2026; Witstok et al. 2026). To remedy this potential bias, in addition to choosing an upper redshift boundary of $z_{\text{phot}} = 14$, we allow the redshift selections described above to be satisfied either under the default approach in Hainline et al. (2026; i.e. using the standard IGM treatment in eazy), or for redshifts obtained with the empirical Asada et al. (2025) prescription.

On the other hand, strong Ly α emission in principle can also cause photometric redshifts to be underestimated (e.g. Wu et al. 2026). Taking $\text{EW}_{\text{Ly}\alpha} = 66 \text{ \AA}$ as in GS-z13-1-LA as an example, the line effectively adds $0.09 \mu\text{m}$ of continuum bluewards of the true Ly α break, which decreases the photometric redshift by $\Delta z = (0.09 \mu\text{m} / \lambda_{\text{Ly}\alpha}) = 0.8$. While many eazy template sets include Ly α emission, additional systematic uncertainty on redshift is introduced when the true Ly α flux significantly deviates from the template, as also remarked by Robertson et al. (2024) even before the spectroscopic confirmation of GS-z13-1-LA.

Overall, we find the selection procedure to generally be robust against minor changes in the selection criteria. Interestingly, we retrieve 16 candidates that are clustered within an angular separation of $\lesssim 6'$ from GS-z13-1-LA. This translates to a projected distance of just over 1 pMpc, similar to the structure reported in Wu et al. (2026). By virtue of the initial selection in Hainline et al. (2026), the best-fit photometric redshift solution is statistically preferred over any $z < 7$ solution ($\Delta\chi^2 > 4$), but we have furthermore verified for each of the 16 candidates that filters bluewards of Ly α do not contain significant detections ($p > 0.1$ under the null hypothesis of zero flux in all filters). The NIRCcam IDs, coordinates, redshifts, UV magnitudes and slopes of these candidates, as inferred by Hainline et al. (2026), can be found in Section C.

The spatial distribution and NIRCcam photometry of these candidates are shown in Fig. 4. Perhaps most strikingly, the brightest candidate (ID 45716) shows a tentative flux excess in the F182M medium-band filter, certainly compared to other candidates such as ID 54533 that show a much smoother break. This filter could contain the Ly α line if it falls slightly redwards compared to GS-z13-1-LA (for which no clear medium-band

photometric boost is observed, since the line falls right between the F162M and F182M filters; W25). As noted in Hainline et al. (2026), this bright galaxy candidate moreover shows an extended, complex morphology, including in F182M. Meanwhile, ID 11457 was already identified in Hainline et al. (2024b), Robertson et al. (2024), and Whitler et al. (2025) as a compact $z \approx 13$ galaxy candidate similar to GS-z13-1-LA, if ever so slightly fainter.

Apart from the 16 nearby photometric candidates, it is further worth mentioning that the spectroscopically confirmed galaxy JADES-GS-z13-0 (Robertson et al. 2023; Curtis-Lake et al. 2023; Hainline et al. 2024a) is found at 8.2' from GS-z13-1-LA (1.7 pMpc). While the continuum break of this source initially suggested $z_{\text{break}} = 13.2$, as discussed above this may be overestimated by up to $\Delta z \approx 0.5$ due to the effects of DLA absorption (Witstok et al. 2026). Indeed, based on a deeper (56 h) spectrum Hainline et al. (2024a) reported a more conservative redshift estimate of $z_{\text{spec}} = 13.13^{+0.09}_{-0.13}$ when taking into account potential DLA absorption, and tentative emission-line detections yielding $z_{\text{spec}} \approx 12.9$ have been found (Hainline et al. 2024a; Pollock et al. 2026), which would place GS-z13-0 close to the redshift of GS-z13-1-LA.

We now turn to evaluate whether the presence of a larger ionised bubble, of the order of $R_{\text{ion}} \approx 0.5$ pMpc (Section 3.2.2), is feasible. As a starting point, we adopt the best-fit Schechter function to the UV luminosity function (UVLF) derived by Whitler et al. (2025) as broadly representative of the current literature consensus (e.g. Finkelstein et al. 2023; Harikane et al. 2023, 2024; Pérez-González et al. 2023; Leung et al. 2023; Hainline et al. 2024b; Robertson et al. 2024; Adams et al. 2024; Donnan et al. 2024). This particular UVLF from Whitler et al. (2025) was based on number counts of F150W dropouts, whose median redshift corresponds to $z = 12.8$. While the conversion of the UVLF into an ionising photon density \dot{n}_{ion} hinges on several key assumptions, we aim to obtain a conservatively high estimate here. We integrate the UVLF down to an absolute UV magnitude of $M_{\text{UV, lim}} = -13$ mag ($M_{\text{UV, lim}} = -15$ mag would reduce \dot{n}_{ion} by approximately 2 \times), consider an average ionising-photon production efficiency of $\xi_{\text{ion}} = 10^{25.5}$ Hz erg $^{-1}$ (higher by a factor of several compared to Simmonds et al. 2024 and Pahl et al. 2025, though perhaps more appropriate for fainter systems; Atek et al. 2024), and assume a relatively high average LyC escape fraction of $f_{\text{esc, LyC}} = 20\%$ (e.g. Robertson 2022 and references therein). These assumptions yield a value of $\dot{n}_{\text{ion}} \approx 2 \times 10^{50}$ s $^{-1}$ cMpc $^{-3}$, yet even such a high rate falls short of ionising a spherical volume with radius $R_{\text{ion}} \approx 0.5$ pMpc within the entire lifetime of the Universe at $z = 13$.

Given the tentatively overdense environment of GS-z13-1-LA, however, the ionised bubble growth could be sped up considerably: a $\gtrsim 3\times$ enhancement of the galaxy density compared to the average field, as deduced for the overdensity identified by Wu et al. (2026; 4 \times in that case), could bring down the bubble formation timescale to the order of 100 Myr or less. Indeed, the confirmed presence of GS-z13-1-LA itself already implies its immediate surroundings are expected to be biased, given the high degree of clustering of galaxies particularly at $z \gtrsim 10$ (e.g. Muñoz et al. 2023; Gelli et al. 2024). While we rely on small number statistics here, a first-order estimate suggests a number density enhancement of a factor of a few is certainly plausible. Over a 1 mag range in M_{UV} we would expect $N_{\text{exp}} \approx 0.4^{+0.4}_{-0.3}$ (5^{+5}_{-3}) galaxies within a sphere with a 0.5 pMpc (1 pMpc) radius, whereas we observe $N_{\text{obs}} = 5$ (14) candidates within consistent projected distances of GS-z13-1-LA (including itself).

Altogether this leads us to conclude that it is feasible for GS-z13-1-LA and its neighbouring galaxies to collectively inhabit a relatively large ionised bubble. However, this hinges on several optimistic assumptions: the ionising photon rate is derived using high estimates of ξ_{ion} and $f_{\text{esc, LyC}}$, and the photometric candidates all require spectroscopic confirmation. Furthermore, we note that an overdense region is not only expected to linearly increase the production rate of ionising photons, but also to cause a local enhancement in the gas density (e.g. Keating et al. 2024b; Kist et al. 2025). This effect will inhibit the formation of an ionised region in a non-linear manner, since the recombination rate scales quadratically with density. Hence, it is unclear if an overdense environment at such an early stage of reionisation augments Ly α transmission or not. A critical test for the scenario with a galaxy overdensity will therefore be to search for additional Ly α emission lines in nearby sources such as the candidates identified in Fig. 4.

Either way, this does not take away from the deduction that GS-z13-1-LA itself should be a prolific producer of ionising photons, a significant fraction of which may be escaping the galaxy, given the extremely blue continuum that allows little room for reprocessing into a redder nebular continuum (Section 4.1). Whether or not a larger bubble is confirmed in the future, the conclusion therefore stands that early galaxies such as GS-z13-1-LA can be extremely efficient ionising agents, and that reionisation was likely underway at $z \approx 13$.

5. Conclusions

We have presented new JWST/NIRSpec spectroscopy of GS-z13-1-LA. Our main findings can be summarised as follows:

- We have combined new, deep NIRSpec/PRISM observations from the OASIS programme (Looser et al. in prep.) with the now completed JADES observations, which with a total of 56 h has tripled the total exposure time compared to W25. This reaffirms the Ly α line detection and the blue UV continuum observed previously, although the OASIS spectrum suggests a less pronounced downturn of the continuum near Ly α . Deeper medium-resolution observations do not reveal a significant line detection, yet remain compatible with the PRISM measurements if the line is spectrally resolved.
- Detailed spectral modelling of the line and continuum emission generally supports the findings from W25, except perhaps the previously inferred large H I column density. A minor wavelength discrepancy in the blue NIRSpec coverage ($\lambda_{\text{obs}} \lesssim 2 \mu\text{m}$) can be explained by small remaining calibration systematics for spatially compact sources near the edges of micro-shutters, urging caution with PRISM-derived measurements in those cases.
- We investigated the implications of the measured Ly α line strength and steep continuum slope, which again point towards GS-z13-1-LA hosting an ionising source with a high effective temperature ($T \gtrsim 60\,000$ K), and allows at most a modest contribution from the nebular continuum. Combined, this implies that ionising photons may escape GS-z13-1-LA at a sufficient rate to lead to the formation of a small ionised bubble ($R_{\text{ion}} \approx 0.2$ pMpc).
- Based on the photometric candidates identified by Hainline et al. (2026), we also identified 16 nearby photometric candidates that together could plausibly establish a larger bubble ($R_{\text{ion}} \approx 0.5$ pMpc). This could alleviate the required ionising production efficiency of GS-z13-1-LA from $\xi_{\text{ion}} \approx 10^{26.4}$ Hz erg $^{-1}$ down to $\approx 10^{25.9}$ Hz erg $^{-1}$, but it

would equally require a notable overdensity of galaxies with highly efficient ionising capabilities.

We conclude that the new observations presented here confirm the overall picture of GS-z13-1-LA as a remarkably powerful ionising source. Observed just 330 Myr after the Big Bang, it provides compelling evidence to extend the timeline of cosmic reionisation towards perhaps unexpectedly early times. Upcoming observations, including a Cycle-4 JWST programme (PID 9016, PI: D. Stark) obtaining deep NIRSpec/G235M spectroscopy and a Cycle 12 ALMA programme (2025.1.00147.S, PI: J. Witstok) targeting the [O III] 88 μ m line, will help further unveil a more detailed picture of what may be the earliest stages of reionisation.

Acknowledgements. We thank Andrea Ferrara, Joshua Cohon, and Charlotte Mason for insightful discussions. This work is based on observations made with the National Aeronautics and Space Administration (NASA)/European Space Agency (ESA)/Canadian Space Agency (CSA) JWST. The data were obtained from the Mikulski Archive for Space Telescopes at the STScI, which is operated by the Association of Universities for Research in Astronomy, Inc., under NASA contract NAS 5-03127 for JWST. These observations are associated with programmes 1180, 1210, 1287, 3215, and 5997. JW and AJC gratefully acknowledge support from the Cosmic Dawn Center through the DAWN Fellowship. The Cosmic Dawn Center (DAWN) is funded by the Danish National Research Foundation under grant No. 140. SC acknowledges support by European Union’s HE European Research Council (ERC) Starting Grant “WINGS” (Grant agreement No. 101040227). AJB acknowledges funding from the “FirstGalaxies” Advanced Grant from the ERC under the European Union’s Horizon 2020 research and innovation programme (No. 789056). FDE, GCJ, RM, and JS acknowledge support by the Science and Technology Facilities Council (STFC), by the ERC through Advanced Grant “QUENCH” (No. 695671), and by the UK Research and Innovation (UKRI) Frontier Research grant RISEandFALL. JMH, BER, BDJ, and CNAW are supported by the JWST/NIRCam Science Team contract to the University of Arizona, NAS5-02105, along with JWST programmes 3215 (JMH, BER, and BDJ) and 8544 (JMH). TJL gratefully acknowledges support from the Swiss National Science Foundation through a SNSF Mobility Fellowship and from the NASA/JWST programme OASIS (PID 5997). WMB gratefully acknowledges support from DARK via the DARK fellowship. This work was supported by a research grant (VIL54489) from VILLUM FONDEN. RM also acknowledges funding from a research professorship from the Royal Society. ST acknowledges support by the Royal Society Research Grant G125142. This work has relied on the following PYTHON packages: the SCIPY library (Jones et al. 2001), its packages NUMPY (Van der Walt et al. 2011) and MATPLOTLIB (Hunter 2007), ASTROPY (Astropy Collaboration et al. 2013, 2018), EMCEE (Foreman-Mackey et al. 2013), FORCEPHO, and (PY)MULTINEST (Feroz et al. 2009; Buchner et al. 2014).

References

Adams, N. J., Conselice, C. J., Austin, D., et al. 2024, *ApJ*, 965, 169
 Algera, H. S. B., Weaver, J. R., Bakx, T. J. L. C., et al. 2025, arXiv e-prints, arXiv:2512.14486
 Alves de Oliveira, C., Birkmann, S. M., Böker, T., et al. 2018, in *Society of Photo-Optical Instrumentation Engineers (SPIE) Conference Series*, Vol. 10704, *Observatory Operations: Strategies, Processes, and Systems VII*, 107040Q
 Asada, Y., Desprez, G., Willott, C. J., et al. 2025, *ApJ*, 983, L2
 Astropy Collaboration, Price-Whelan, A. M., Sipőcz, B. M., et al. 2018, *AJ*, 156, 123
 Astropy Collaboration, Robitaille, T. P., Tollerud, E. J., et al. 2013, *A&A*, 558, A33
 Atek, H., Chemerynska, I., Wang, B., et al. 2023, *MNRAS*, 524, 5486
 Atek, H., Labbé, I., Furtak, L. J., et al. 2024, *Nature*, 626, 975
 Austin, D., Conselice, C. J., Adams, N. J., et al. 2025, *ApJ*, 995, 43
 Baker, W. M., D’Eugenio, F., Maiolino, R., et al. 2025a, *A&A*, 697, A90
 Baker, W. M., Tacchella, S., Johnson, B. D., et al. 2025b, *Nature Astronomy*, 9, 141
 Bera, A., Hassan, S., Feldmann, R., Davé, R., & Finlator, K. 2025, arXiv e-prints, arXiv:2511.19600
 Bhagwat, A., Napolitano, L., Pentericci, L., Ciardi, B., & Costa, T. 2025, *MNRAS*, 542, 128
 Bosman, S. E. I., Davies, F. B., Becker, G. D., et al. 2022, *MNRAS*, 514, 55
 Brammer, G. B., van Dokkum, P. G., & Coppi, P. 2008, *ApJ*, 686, 1503
 Buchner, J., Georgakakis, A., Nandra, K., et al. 2014, *A&A*, 564, A125
 Bunker, A. J., Cameron, A. J., Curtis-Lake, E., et al. 2024, *A&A*, 690, A288
 Bunker, A. J., Saxena, A., Cameron, A. J., et al. 2023, *A&A*, 677, A88

Bunker, A. J., Stanway, E. R., Ellis, R. S., McMahon, R. G., & McCarthy, P. J. 2003, *MNRAS*, 342, L47
 Cain, C., Van Engelen, A., Croker, K. S., et al. 2025, *ApJ*, 987, L29
 Cameron, A. J., Katz, H., Witten, C., et al. 2024, *MNRAS*, 534, 523
 Carniani, S., D’Eugenio, F., Ji, X., et al. 2025, *A&A*, 696, A87
 Carniani, S., Hainline, K., D’Eugenio, F., et al. 2024, *Nature*, 633, 318
 Chen, Z., Stark, D. P., Mason, C. A., et al. 2025, arXiv e-prints, arXiv:2505.24080
 Cohon, J., Cain, C., Windhorst, R., et al. 2025, arXiv e-prints, arXiv:2508.05739
 Cooper, O. R., Casey, C. M., Akins, H. B., et al. 2024, *ApJ*, 970, 50
 Crowther, P. A. 2007, *ARA&A*, 45, 177
 Cullen, F., McLeod, D. J., McLure, R. J., et al. 2024, *MNRAS*, 531, 997
 Cullen, F., McLure, R. J., McLeod, D. J., et al. 2023, *MNRAS*, 520, 14
 Curti, M., Witstok, J., Jakobsen, P., et al. 2025, *A&A*, 697, A89
 Curtis-Lake, E., Cameron, A. J., Bunker, A. J., et al. 2025, arXiv e-prints, arXiv:2510.01033
 Curtis-Lake, E., Carniani, S., Cameron, A., et al. 2023, *Nature Astronomy*, 7, 622
 Dayal, P. & Ferrara, A. 2018, *Phys. Rep.*, 780, 1
 de Graaff, A., Brammer, G., Weibel, A., et al. 2025, *A&A*, 697, A189
 de Lera Acedo, E., de Villiers, D. I. L., Razavi-Ghods, N., et al. 2022, *Nature Astronomy*, 6, 984
 D’Eugenio, F., Cameron, A. J., Scholtz, J., et al. 2025a, *ApJS*, 277, 4
 D’Eugenio, F., Maiolino, R., Carniani, S., et al. 2024, *A&A*, 689, A152
 D’Eugenio, F., Nelson, E. J., Eisenstein, D. J., et al. 2025b, arXiv e-prints, arXiv:2510.11626
 Donnan, C. T., McLeod, D. J., McLure, R. J., et al. 2026, arXiv e-prints, arXiv:2601.15151
 Donnan, C. T., McLure, R. J., Dunlop, J. S., et al. 2024, *MNRAS*, 533, 3222
 Eisenstein, D. J., Johnson, B. D., Robertson, B., et al. 2025, *ApJS*, 281, 50
 Eisenstein, D. J., Willott, C., Alberts, S., et al. 2026, *ApJS*, 283, 6
 Endsley, R. & Stark, D. P. 2022, *MNRAS*, 511, 6042
 Erb, D. K., Steidel, C. C., Trainor, R. F., et al. 2014, *ApJ*, 795, 33
 Feroz, F., Hobson, M. P., & Bridges, M. 2009, *MNRAS*, 398, 1601
 Ferruit, P., Jakobsen, P., Giardino, G., et al. 2022, *A&A*, 661, A81
 Finkelstein, S. L., Bagley, M. B., Ferguson, H. C., et al. 2023, *ApJ*, 946, L13
 Finkelstein, S. L., Papovich, C., Dickinson, M., et al. 2013, *Nature*, 502, 524
 Foreman-Mackey, D., Hogg, D. W., Lang, D., & Goodman, J. 2013, *PASP*, 125, 306
 Fujimoto, S., Arrabal Haro, P., Dickinson, M., et al. 2023, *ApJ*, 949, L25
 Fujimoto, S., Wang, B., Weaver, J. R., et al. 2024, *ApJ*, 977, 250
 Gelli, V., Mason, C., & Hayward, C. C. 2024, *ApJ*, 975, 192
 Gelli, V., Mason, C., Pallottini, A., et al. 2025, arXiv e-prints, arXiv:2510.01315
 Göteborg, Y., de Mink, S. E., & Groh, J. H. 2017, *A&A*, 608, A11
 Hainline, K. N., D’Eugenio, F., Jakobsen, P., et al. 2024a, *ApJ*, 976, 160
 Hainline, K. N., Eisenstein, D. J., Whitler, L., et al. 2026, arXiv e-prints, arXiv:2601.15959
 Hainline, K. N., Johnson, B. D., Robertson, B., et al. 2024b, *ApJ*, 964, 71
 Harikane, Y., Nakajima, K., Ouchi, M., et al. 2024, *ApJ*, 960, 56
 Harikane, Y., Ouchi, M., Oguri, M., et al. 2023, *ApJS*, 265, 5
 Hayes, M. J., Runnholm, A., Gronke, M., & Scarlata, C. 2021, *ApJ*, 908, 36
 Heintz, K. E., Brammer, G. B., Watson, D., et al. 2025a, *A&A*, 693, A60
 Heintz, K. E., Pollock, C. L., Witstok, J., et al. 2025b, *ApJ*, 987, L2
 Heintz, K. E., Watson, D., Brammer, G., et al. 2024, *Science*, 384, 890
 Helton, J. M., Sun, F., Woodrum, C., et al. 2024a, *ApJ*, 962, 124
 Helton, J. M., Sun, F., Woodrum, C., et al. 2024b, *ApJ*, 974, 41
 Hu, W., Martin, C. L., Gronke, M., et al. 2023, *ApJ*, 956, 39
 Huberty, M., Scarlata, C., Hayes, M. J., & Gazagnes, S. 2025, *ApJ*, 987, 82
 Hunter, J. D. 2007, *Computing in Science & Engineering*, 9, 90
 Hviding, R. E., de Graaff, A., Miller, T. B., et al. 2025, *A&A*, 702, A57
 Jakobsen, P., Ferruit, P., Alves de Oliveira, C., et al. 2022, *A&A*, 661, A80
 Jecmen, M. C., Chisholm, J., Atek, H., et al. 2026, arXiv e-prints, arXiv:2601.19995
 Johnson, B. D., Robertson, B. E., Eisenstein, D. J., et al. 2026, arXiv e-prints, arXiv:2601.15954
 Jones, E., Oliphant, T., Peterson, P., et al. 2001, *SciPy: Open source scientific tools for Python*, [Online; accessed <today>]
 Jones, G. C., Bunker, A. J., Saxena, A., et al. 2024, *A&A*, 683, A238
 Kageura, Y., Ouchi, M., Nakane, M., et al. 2025, *ApJS*, 278, 33
 Katz, H., Cameron, A. J., Saxena, A., et al. 2025, *The Open Journal of Astrophysics*, 8, 104
 Keating, L. C., Bolton, J. S., Cullen, F., et al. 2024a, *MNRAS*, 532, 1646
 Keating, L. C., Puchwein, E., Bolton, J. S., Haehnelt, M. G., & Kulkarni, G. 2024b, *MNRAS*, 531, L34
 Kist, T., Hennawi, J. F., & Davies, F. B. 2025, *MNRAS*, 544, 2316
 Larson, R. L., Finkelstein, S. L., Hutchison, T. A., et al. 2022, *ApJ*, 930, 104
 Leclercq, F., Bacon, R., Verhamme, A., et al. 2020, *A&A*, 635, A82
 Leonova, E., Naidu, R. P., Oesch, P. A., et al. 2025, arXiv e-prints, arXiv:2512.06072
 Leung, G. C. K., Bagley, M. B., Finkelstein, S. L., et al. 2023, *ApJ*, 954, L46
 Lu, T.-Y., Mason, C. A., Hutter, A., et al. 2024, *MNRAS*, 528, 4872
 Luridiana, V., Morisset, C., & Shaw, R. A. 2015, *A&A*, 573, A42

- Marques-Chaves, R., Álvarez-Márquez, J., Colina, L., et al. 2026, arXiv e-prints, arXiv:2602.02322
- Martin, C. L., Hu, W., Wold, I. G. B., et al. 2026, *ApJ*, 997, 102
- Martins, F. & Palacios, A. 2022, *A&A*, 659, A163
- Mason, C. A., Chen, Z., Stark, D. P., et al. 2026, *A&A*, 705, A114
- Mason, C. A., Treu, T., Dijkstra, M., et al. 2018, *ApJ*, 856, 2
- Meiksin, A. A. 2009, *Reviews of Modern Physics*, 81, 1405
- Muñoz, J. B., Mirocha, J., Furlanetto, S., & Sabti, N. 2023, *MNRAS*, 526, L47
- Naidu, R. P., Oesch, P. A., Brammer, G., et al. 2026, *The Open Journal of Astrophysics*, 9, 56033
- Napolitano, L., Pentericci, L., Dickinson, M., et al. 2025, arXiv e-prints, arXiv:2508.14171
- Navarro-Carrera, R., Caputi, K. I., Iani, E., et al. 2025, *ApJ*, 993, 194
- Neyer, M., Smith, A., Kannan, R., et al. 2024, *MNRAS*, 531, 2943
- Neyer, M., Smith, A., Vogelsberger, M., et al. 2025, arXiv e-prints, arXiv:2510.18946
- Oesch, P. A., van Dokkum, P. G., Illingworth, G. D., et al. 2015, *ApJ*, 804, L30
- Oke, J. B. & Gunn, J. E. 1983, *ApJ*, 266, 713
- Ono, Y., Ouchi, M., Mobasher, B., et al. 2012, *ApJ*, 744, 83
- Ouchi, M., Ono, Y., & Shibuya, T. 2020, *ARA&A*, 58, 617
- Pahl, A., Topping, M. W., Shapley, A., et al. 2025, *ApJ*, 981, 134
- Pentericci, L., Vanzella, E., Castellano, M., et al. 2018, *A&A*, 619, A147
- Pérez-González, P. G., Costantin, L., Langeroodi, D., et al. 2023, *ApJ*, 951, L1
- Planck Collaboration, Aghanim, N., Akrami, Y., et al. 2020, *A&A*, 641, A6
- Pollock, C. L., Heintz, K. E., Witstok, J., et al. 2026, arXiv e-prints, arXiv:2602.11783
- Prieto-Lyon, G., Mason, C. A., Strait, V., et al. 2025, arXiv e-prints, arXiv:2509.18302
- Qin, Y., Mesinger, A., Prelogović, D., et al. 2025, *PASA*, 42, e049
- Qin, Y. & Wyithe, J. S. B. 2025, *MNRAS*, 538, L16
- Rieke, M. J., Kelly, D. M., Misselt, K., et al. 2023a, *PASP*, 135, 028001
- Rieke, M. J., Robertson, B., Tacchella, S., et al. 2023b, *ApJS*, 269, 16
- Roberts-Borsani, G. W., Bouwens, R. J., Oesch, P. A., et al. 2016, *ApJ*, 823, 143
- Robertson, B., Johnson, B. D., Tacchella, S., et al. 2024, *ApJ*, 970, 31
- Robertson, B. E. 2022, *ARA&A*, 60, 121
- Robertson, B. E., Johnson, B. D., Tacchella, S., et al. 2026, arXiv e-prints, arXiv:2601.15956
- Robertson, B. E., Tacchella, S., Johnson, B. D., et al. 2023, *Nature Astronomy*, 7, 611
- Runnholm, A., Hayes, M. J., Mehta, V., et al. 2025, *ApJ*, 984, 95
- Sailer, N., Farren, G. S., Ferraro, S., & White, M. 2026, *Phys. Rev. Lett.*, 136, 081002
- Saxena, A., Bunker, A. J., Jones, G. C., et al. 2024a, *A&A*, 684, A84
- Saxena, A., Cameron, A. J., Katz, H., et al. 2024b, arXiv e-prints, arXiv:2411.14532
- Saxena, A., Robertson, B. E., Bunker, A. J., et al. 2023, *A&A*, 678, A68
- Scholtz, J., Carniani, S., Parlanti, E., et al. 2025, arXiv e-prints, arXiv:2510.01034
- Scholtz, J., Witten, C., Laporte, N., et al. 2024, *A&A*, 687, A283
- Shakura, N. I. & Sunyaev, R. A. 1973, *A&A*, 24, 337
- Simmonds, C., Tacchella, S., Hainline, K., et al. 2024, *MNRAS*, 535, 2998
- Smit, R., Swinbank, A. M., Massey, R., et al. 2017, *MNRAS*, 467, 3306
- Spitzer, Jr., L. & Greenstein, J. L. 1951, *ApJ*, 114, 407
- Steidel, C. C., Rudie, G. C., Strom, A. L., et al. 2014, *ApJ*, 795, 165
- Tacchella, S., Eisenstein, D. J., Hainline, K., et al. 2023, *ApJ*, 952, 74
- Tang, M., Stark, D. P., Chen, Z., et al. 2023, *MNRAS*, 526, 1657
- Tang, M., Stark, D. P., Ellis, R. S., et al. 2024a, *MNRAS*, 531, 2701
- Tang, M., Stark, D. P., Ellis, R. S., et al. 2024b, *ApJ*, 972, 56
- Tang, M., Stark, D. P., Topping, M. W., Mason, C., & Ellis, R. S. 2024c, *ApJ*, 975, 208
- Topping, M. W., Stark, D. P., Endsley, R., et al. 2024, *MNRAS*, 529, 4087
- Villasenor, B., Robertson, B., Madau, P., & Schneider, E. 2022, *ApJ*, 933, 59
- van der Walt, S., Colbert, S. C., & Varoquaux, G. 2011, *Computing in Science and Engineering*, 13, 22
- Whitler, L., Stark, D. P., Topping, M. W., et al. 2025, *ApJ*, 992, 63
- Willott, C. J., Asada, Y., Iyer, K. G., et al. 2025, *ApJ*, 988, 26
- Witstok, J., Jakobsen, P., Maiolino, R., et al. 2025a, *Nature*, 639, 897
- Witstok, J., Maiolino, R., Smit, R., et al. 2025b, *MNRAS*, 536, 27
- Witstok, J., Smit, R., Baker, W. M., et al. 2026, *The Open Journal of Astrophysics*, 9, 55261
- Witstok, J., Smit, R., Maiolino, R., et al. 2021, *MNRAS*, 508, 1686
- Witstok, J., Smit, R., Saxena, A., et al. 2024, *A&A*, 682, A40
- Wu, S., Shi, X., Kalita, N., et al. 2024, *MNRAS*, 532, 4703
- Wu, Z., Eisenstein, D. J., Johnson, B. D., et al. 2026, arXiv e-prints, arXiv:2601.15960
- Wu, Z., Eisenstein, D. J., Johnson, B. D., et al. 2025, *ApJ*, 992, 212
- Yanagisawa, H., Ouchi, M., Nakajima, K., et al. 2025, *ApJ*, 988, 86
- Yuan, Y., Martín-Alvarez, S., Haehnelt, M. G., et al. 2025, *MNRAS*, 542, 762
- Zhu, Y., Becker, G. D., Bosman, S. E. I., et al. 2022, *ApJ*, 932, 76
- Zitrin, A., Labbé, I., Belli, S., et al. 2015, *ApJ*, 810, L12

Authors and affiliations

Joris Witstok ^{*1,2}, Stefano Carniani ³, Peter Jakobsen ^{1,2}, Andrew J. Bunker ⁴, Alex J. Cameron ^{1,2},
Francesco D'Eugenio ^{5,6}, Kevin Hainline ⁷, Jakob M. Helton ⁸, Tobias J. Looser ⁹, Pierluigi Rinaldi ¹⁰,
Brant E. Robertson ¹¹, William M. Baker ¹², Stéphane Charlot ¹³, Benjamin D. Johnson ⁹,
Gareth C. Jones ^{5,6}, Nimisha Kumari ¹⁴, Roberto Maiolino ^{5,6,15}, Jan Scholtz ^{5,6}, Sandro Tacchella ^{5,6},
Christopher N. A. Willmer ⁷, Chris Willott ¹⁶, and Zihao Wu ⁹

¹ Cosmic Dawn Center (DAWN), Copenhagen, Denmark

² Niels Bohr Institute, University of Copenhagen, Jagtvej 128, DK-2200, Copenhagen, Denmark

³ Scuola Normale Superiore, Piazza dei Cavalieri 7, I-56126 Pisa, Italy

⁴ Department of Physics, University of Oxford, Denys Wilkinson Building, Keble Road, Oxford OX1 3RH, UK

⁵ Kavli Institute for Cosmology, University of Cambridge, Madingley Road, Cambridge CB3 0HA, UK

⁶ Cavendish Laboratory, University of Cambridge, 19 JJ Thomson Avenue, Cambridge CB3 0HE, UK

⁷ Steward Observatory, University of Arizona, 933 N. Cherry Ave., Tucson, AZ 85721, USA

⁸ Department of Astronomy & Astrophysics, The Pennsylvania State University, University Park, PA 16802, USA

⁹ Center for Astrophysics | Harvard & Smithsonian, 60 Garden St., Cambridge, MA 02138, USA

¹⁰ Space Telescope Science Institute, 3700 San Martin Drive, Baltimore, MD 21218, USA

¹¹ Department of Astronomy and Astrophysics University of California, Santa Cruz, 1156 High Street, Santa Cruz, CA 96054, USA

¹² DARK, Niels Bohr Institute, University of Copenhagen, Jagtvej 155A, DK-2200 Copenhagen, Denmark

¹³ Sorbonne Université, CNRS, UMR 7095, Institut d'Astrophysique de Paris, 98 bis bd Arago, 75014 Paris, France

¹⁴ AURA for European Space Agency, Space Telescope Science Institute, 3700 San Martin Drive, Baltimore, MD 21210, USA

¹⁵ Department of Physics and Astronomy, University College London, Gower Street, London WC1E 6BT, UK

¹⁶ NRC Herzberg, 5071 West Saanich Rd, Victoria, BC V9E 2E7, Canada

* E-mail: joris.witstok@nbi.ku.dk

Appendix A: Two-dimensional NIRSpec/PRISM spectra and NIRSpec/G235M observations

In Fig. A.1, the two-dimensional and one-dimensional NIRSpec/PRISM spectra are shown both in the default reduction where all three nod positions are considered, and in the case where only the two outer nod positions are considered (leading to reduced SNR but avoiding potential self-subtraction). In Fig. A.2, we show the combined NIRSpec/G235M spectra from JADES and the DSS survey as part of PID 3215 (Section 2.1).

10 **Appendix B: Full spectral model posterior**

In Fig. B.1, we show the full posterior distributions of the fiducial spectral model (Section 3.2).

Appendix C: Photometric candidates

In Table C.1, we list the 16 photometric candidates and 1 spectroscopically confirmed source (JADES-GS-z13-0; Robertson et al. 2023; Curtis-Lake et al. 2023; Hainline et al. 2024a) found in the vicinity of GS-z13-1-LA (Section 4.2).

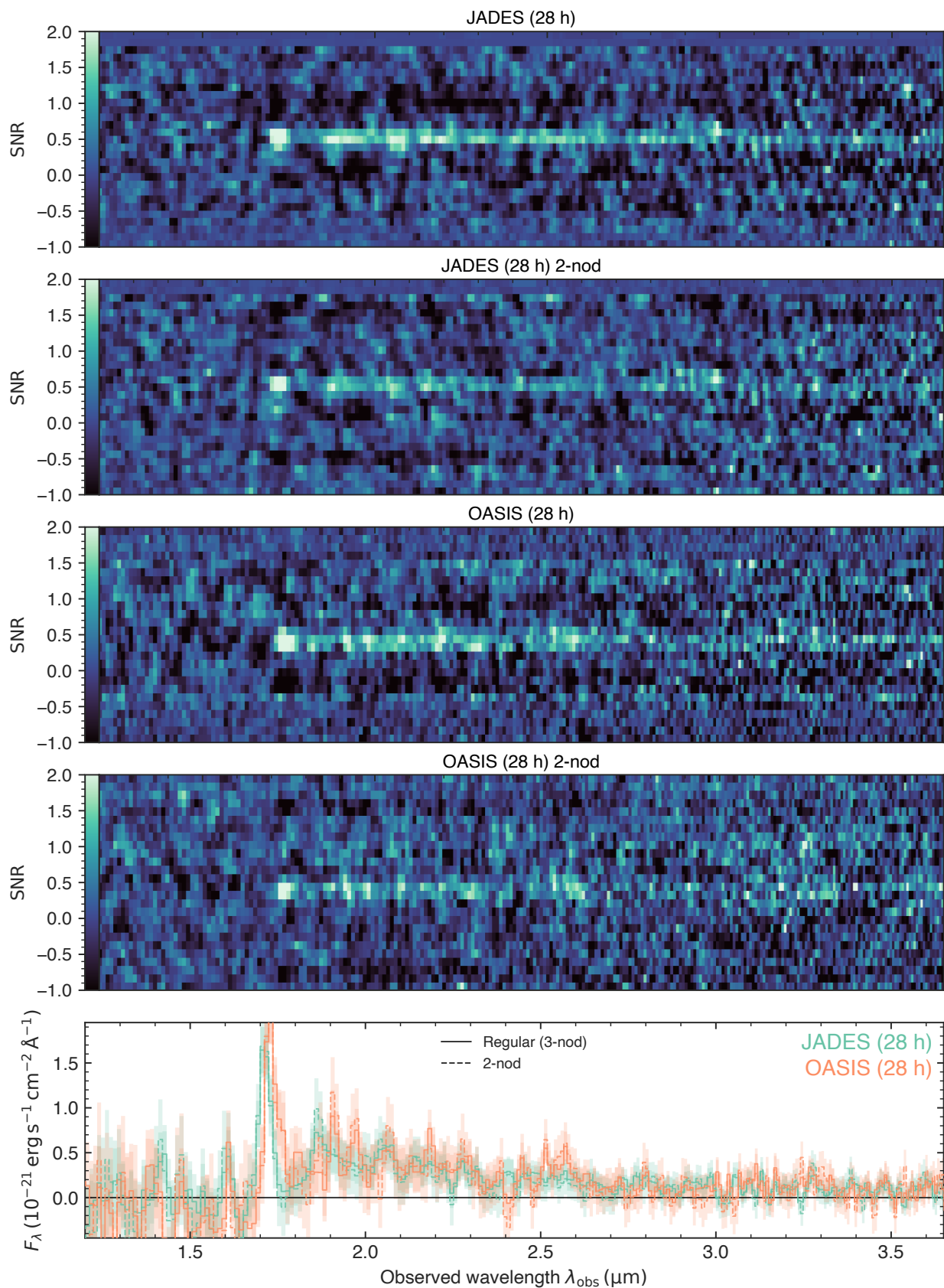


Fig. A.1. Two-dimensional spectra from JADES and OASIS, both in the default reduction where all three nod positions are considered ('3-nod'), and in the case where only the two outer nod positions are considered ('2-nod', leading to reduced SNR but avoiding potential self-subtraction). The line and continuum emission is observed to be spatially compact. The bottom panel further shows little difference between one-dimensional spectra extracted in the two reductions, suggesting that the effect of self-subtraction is limited.

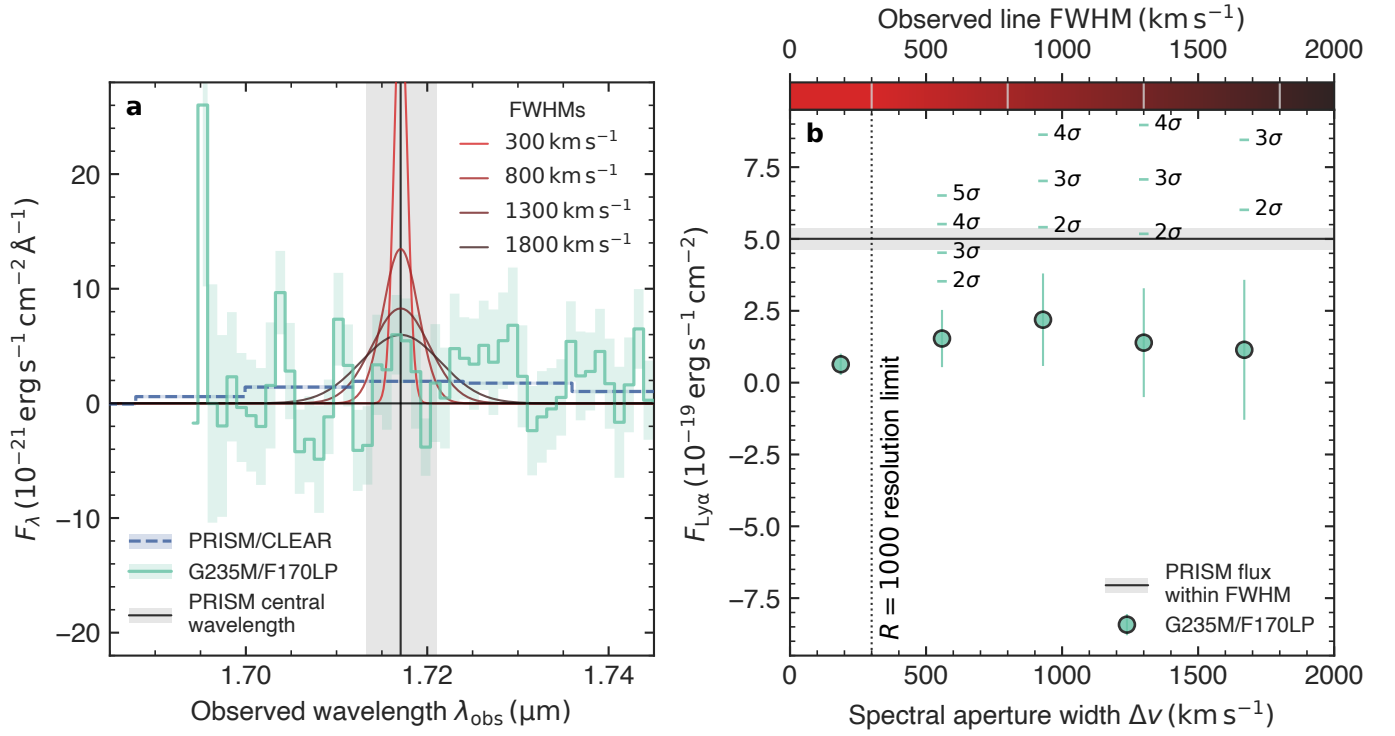


Fig. A.2. a, Combined NIRSPEC/G235M spectroscopy from JADES and the DSS survey as part of PID 3215 (Section 2.1). Modelled Ly α emission-line profiles (solid curves) with matched flux and central wavelength (vertical black line) to the PRISM measurements are shown at different values of the FWHM according to legend and the grey vertical lines in the colourbar in panel b, increasing from the $R = 1000$ resolution limit. **b,** Inferred G235M Ly α flux in an incrementally widened spectral aperture (circles), none of which show a significant detection. The fraction of the PRISM line flux that would be contained within the FWHM of a Gaussian profile (76%) is indicated by the horizontal black line and grey shading, while the $R = 1000$ resolution is shown by a vertical dotted line. If the Ly α line is intrinsically broad (FWHM $\gtrsim 600$ km s $^{-1}$), the current measurements are not strongly in tension ($\lesssim 2\sigma$; cf. annotated significance levels).

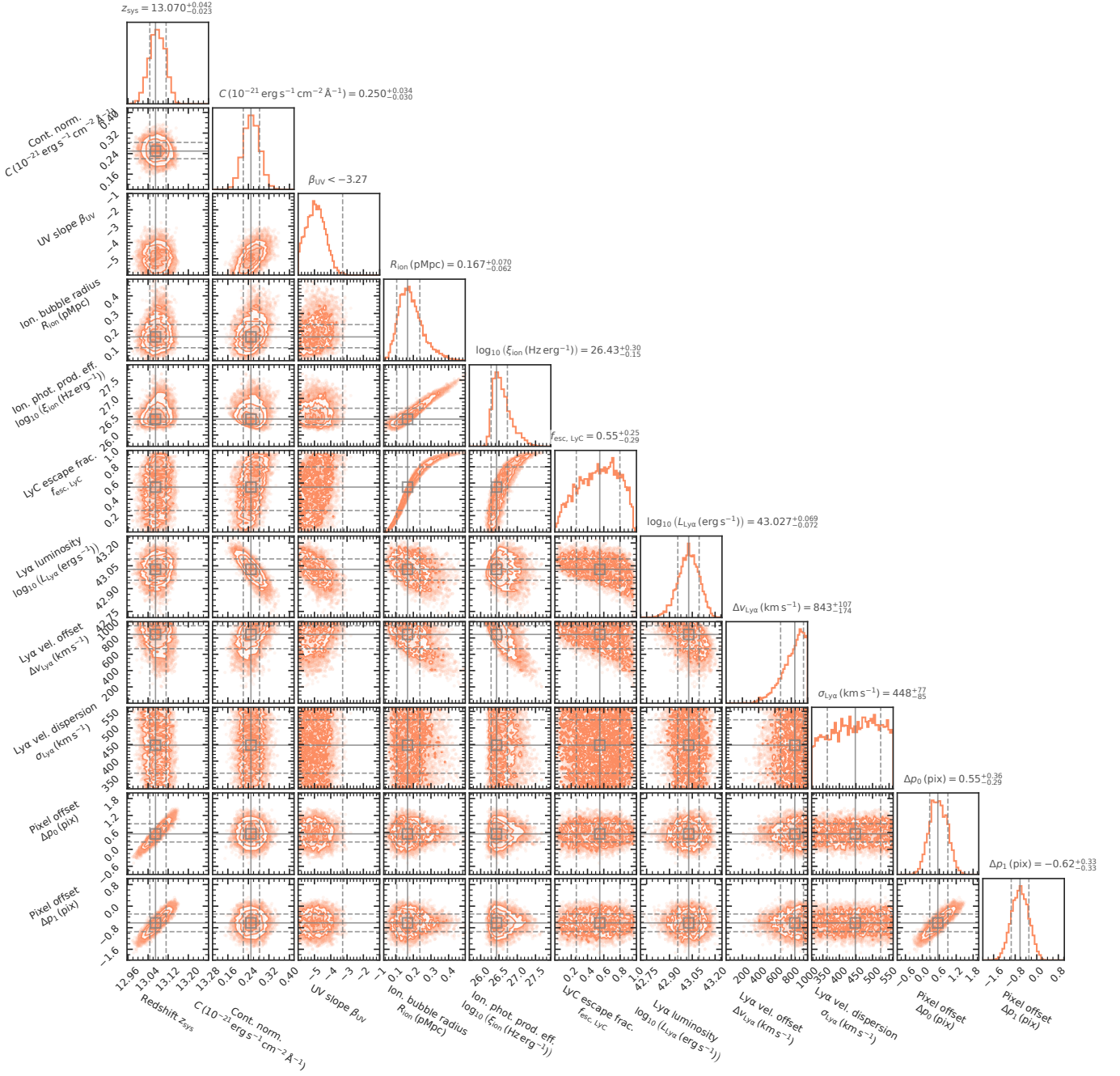


Fig. B.1. Posterior distributions obtained from spectral modelling of the PRISM spectrum of GS-z13-1-LA (Section 3.2). Individual panels show the inter-dependencies between the 9 free parameters of the model, as well as the derived Ly α luminosity $L_{\text{Ly}\alpha}$ (cf. Table 2).

Table C.1. Photometric candidates identified in [Robertson et al. \(2024\)](#) and [Hainline et al. \(2026\)](#) in the vicinity of GS-z13-1-LA (Section 4.2).

ID	RA (deg)	Dec (deg)	z	z_{DLA}	M_{UV} (mag)	β_{UV}	θ (arcmin)	θ (pMpc)
41223	53.10013	-27.86948	$12.25^{+1.28}_{-1.37}$	$12.11^{+1.16}_{-1.75}$	-17.71 ± 0.13	-1.8 ± 0.5	2.3	0.5
296077	53.033974	-27.880013	$12.33^{+1.86}_{-1.05}$	$12.16^{+1.55}_{-0.96}$	-17.72 ± 0.09	-2.6 ± 0.4	1.7	0.4
354289	53.04021	-27.93045	$12.36^{+1.03}_{-0.95}$	$12.06^{+1.08}_{-0.71}$	-18.00 ± 0.13	-2.9 ± 0.4	2.7	0.6
10346	53.12498	-27.89461	$12.41^{+1.73}_{-1.12}$	$11.95^{+1.54}_{-1.04}$	-18.36 ± 0.12	-2.0 ± 0.4	3.2	0.7
508167	52.996464	-27.85939	$12.59^{+0.97}_{-0.80}$	$11.83^{+0.89}_{-0.82}$	-17.97 ± 0.13	-2.3 ± 0.4	4.1	0.9
343416	53.057137	-27.924593	$12.69^{+1.49}_{-1.27}$	$12.28^{+1.29}_{-1.12}$	-18.16 ± 0.11	-2.1 ± 0.4	2.1	0.4
377520	53.089848	-27.904896	$12.72^{+1.26}_{-1.23}$	$12.37^{+1.12}_{-1.09}$	-18.05 ± 0.10	-2.4 ± 0.4	1.6	0.3
54533	53.129128	-27.860743	$12.78^{+0.30}_{-0.37}$	$12.49^{+0.61}_{-0.32}$	-18.34 ± 0.10	-2.4 ± 0.3	3.8	0.8
52569	53.104687	-27.86187	$12.83^{+0.73}_{-0.61}$	$12.66^{+0.53}_{-0.44}$	-17.76 ± 0.09	-2.4 ± 0.3	2.7	0.6
11457	53.02868	-27.89301	$13.04^{+1.11}_{-0.40}$	$13.41^{+0.58}_{-0.51}$	-18.39 ± 0.06	-1.5 ± 0.3	1.9	0.4
13731*	53.06475	-27.890234	$13.07^{+0.04**}_{-0.02}$	–	-18.44 ± 0.07	$-3.2 \pm 0.3**$	–	–
84402	53.126827	-27.836336	$13.08^{+0.76}_{-0.43}$	$12.53^{+0.50}_{-0.30}$	-17.73 ± 0.21	-2.5 ± 0.7	4.6	1.0
128771 [†]	53.149883	-27.776503	$13.13^{+0.09‡}_{-0.13}$	–	-18.55 ± 0.04	$-2.7 \pm 0.1‡$	8.2	1.7
45716	53.139744	-27.866167	$13.21^{+0.79}_{-0.75}$	$12.19^{+0.78}_{-0.59}$	-18.75 ± 0.07	-1.8 ± 0.4	4.2	0.9
502974	53.14879	-27.942274	$13.43^{+1.01}_{-1.00}$	$12.34^{+0.96}_{-0.81}$	-18.21 ± 0.12	-2.7 ± 0.6	5.4	1.1
535088	53.153336	-27.874805	$13.46^{+0.71}_{-0.84}$	$12.42^{+0.77}_{-0.68}$	-17.70 ± 0.15	-2.0 ± 1.0	4.8	1.0
536773	53.142136	-27.922363	$13.56^{+1.31}_{-1.47}$	$13.28^{+1.23}_{-1.36}$	-18.03 ± 0.11	-1.3 ± 0.6	4.5	1.0
184202	53.11405	-27.854027	$14.86^{+0.67}_{-0.81}$	$13.81^{+0.51}_{-0.60}$	-18.90 ± 0.09	-1.8 ± 0.4	3.4	0.7
275184	53.1224	-27.840427	$14.94^{+0.59}_{-0.73}$	$13.97^{+0.51}_{-0.61}$	-18.00 ± 0.15	-2.9 ± 0.7	4.3	0.9

Notes. Listed properties are the NIRCam ID, right ascension (RA), declination (Dec), photometric redshift both without and with the [Asada et al. \(2025\)](#) DLA prescription (z and z_{DLA} , respectively), absolute UV magnitude (M_{UV}), and UV slope (β_{UV}), as reported in the [Hainline et al. \(2026\)](#) catalogue (except for JADES-GS-z13-0 and GS-z13-1-LA; see footnotes below). Also listed is the (projected) separation θ from GS-z13-1-LA.

(*) GS-z13-1-LA.

(**) Spectroscopic redshift and UV slope obtained in Section 3.2.

(†) JADES-GS-z13-0.

(‡) Spectroscopic redshift (taking into account DLA absorption) and UV slope as inferred by [Hainline et al. \(2024a\)](#).